中央大学博士論文

# Analysis of negative differential conductivity and lifetime of bound states in holographic conductors

**Shuta Ishigaki**
石垣　秀太

博士（理学）

中央大学大学院
理工学研究科
物理学専攻

令和2年度
２０２１年３月

**Abstract**

We clarify the mechanism for negative differential conductivity in holographic conductors. Negative differential conductivity is a phenomenon in which the electric field decreases with the increase of the current. Although this phenomenon is widely observed in strongly correlated insulators, its mechanism is not completely understood so far. One reason of the difficulties is that the system is far from equilibrium. We use the AdS/CFT correspondence to analyze this non-equilibrium phenomenon. It has been known that some gravity model (holographic conductor) reproduces negative differential conductivity. We study the mechanism for negative differential conductivity in holographic conductors by analyzing the lifetime of the bound states of the charge carriers. We find that when the system shows negative differential conductivity, the lifetime of the bound states grows as the electric field increases. This suggests that the negative differential conductivity in this system is realized by the suppression of the ionization of the bound states that supplies the free carriers.

# Contents

# Chapter 1

# Introduction

Negative differential conductivity (NDC) is a phenomenon where the electric field acting on the system decreases as the current increases. Electric devices which exhibit NDC play an important role in construction of switching circuits and oscillator circuits from the viewpoint of electronics. NDC has been observed in a wide range of strongly-correlated electron systems [1]. However, we still lack a complete understanding of the mechanism for NDC on the basis of the microscopic theory.[1] A crucial reason for the difficulty is that we need to deal with physics far from equilibrium.

A system is out of equilibrium in the presence of electric current along the direction of the electric field, since the Joule heating breaks the detailed balance. When the applied electric field is small, we can analyze the response of the system perturbatively: the formalism is referred to as the linear response theory. For example, the conductivity of a system in the Ohmic regime can be computed in the framework of the linear response theory. However, computation of nonlinear conductivity is beyond this method since the perturbative analysis is not valid. Since NDC is a nonlinear phenomena, we need a method beyond the linear response theory.

In this thesis, we consider non-equilibrium steady states (NESSs) with a steady current with a constant electric field. We overcome the difficulties associated with the non-equilibrium systems by using the AdS/CFT correspondence [2–4]. The AdS/CFT correspondence states that a strongly-coupled gauge theory is equivalent to a higher-dimensional supergravity. The AdS/CFT correspondence can be a powerful tool to study non-equilibrium systems, because it allows us to circumvent the difficulties by mapping the quantum gauge theory to the classical gravity theory. Since the AdS/CFT correspondence gives the expectation values of physical quantities directly in the language of gravity, one can compute the expectation values even out of equilibrium by using the AdS/CFT correspondence. Recently, the AdS/CFT correspondence has been applied to analysis of NDC

[1] The NDC of electric devices such as Esaki diode has been explained by the tunneling effect at the p-n junction. However, the NDC we consider is a non-ballistic transport of charged particles in bulk materials.

[5–9]. In Refs. [5–9], the D3-D7 model [10, 11] is employed as a gravity dual of a $(3+1)$-dimensional many-body system of charged particles interacting with a thermal reservoir.[2] It has been found that this model exhibits NDC at low temperatures. However, the mechanism for the NDC in this system has not been understood.

It is known that the system has bound states consisting of a positively charged particle and a negatively charged particle [12]. If we make an analogy with QCD, the bound states correspond to mesons, or bound states of quark and anti-quark. However, it would be more appropriate to make an analogy with strongly-correlated electron systems when our aim is investigation of nonlinear conductivity in materials. In this context, the bound state is regarded as an exciton consisting of an electron and a hole. In this thesis, we study the mechanism of the NDC by analyzing the lifetime of the bound states.[13]

We employ the D3-D7 model with vanishing charge density. The system behaves as an insulator at sufficiently low temperatures. When we apply a large enough electric field to the system, we can break the insulation. This is because the positively-charged particles (which we call positive carriers for short) and the negatively-charged particles (which we call negative carriers) will be created by the Schwinger effect.[3]

However, the neutral bound states do not contribute to the DC charge transport. This implies that the formation of the bound states suppresses the conductivity. With this in mind, we study the relationship between the lifetime of the bound states and the electric field, systematically. In our system, we have three possible origins of the charge carriers which contribute to the conductivity: thermal excitation from the vacuum, pair creation from the vacuum induced by the external electric field, and ionization of the already-existing bound states by the electric field. We will clarify which process is the main contribution to the realization of the NDC.

In the context of the AdS/CFT correspondence, the bound state is realized as modes referred to as quasi normal modes (QNMs) in the gravity theory. The (quasi-)normal frequencies of these modes correspond to the location of the pole of the retarded Green function. The pole of the Green function captures the properties of the bound state. The lifetime of the bound state is read from this (quasi-)normal frequency. We analyze the lowest QNM in the D3-D7 model under the presence of a constant electric field. We investigate the lifetime of the bound state as a function of the constant electric field in this model.

We find a counter-intuitive behavior of the bound states when the system exhibits NDC: the lifetime of the bound states grows as the electric field increases. We also find that the DC conductivity approaches zero when the lifetime of the bound states vanishes when the system shows NDC. This means that the charge carriers in the NDC region are mainly supplied by the decay process of the bound states. This explains the mechanism of NDC well: the larger the electric field, the longer the lifetime of the bound states, then the number density of

[2] The D3-D5 model for $2+1$-dimensional systems is also considered in Ref. [7].

[3] This corresponds to the Landau-Zener effect in solid state physics.

charge carriers decreases and the current density decreases.

We also provide other examples of the applications of the QNM analysis in the D3-D7 model.[14] It has been known the D3-D7 model exhibits the spontaneous breaking of the chiral symmetry under applying external magnetic field.[15, 16] This is holographic realization of the magnetic catalysis in the context of QCD. We investigate the dispersion relations of the Nambu-Goldstone modes appearing with the chiral symmetry breaking in the dissipative system by employing the D3-D7 model. The dispersion relation is also computed by the QNM analysis. We find that the short-length behavior of the dispersion relations agree with the results from the effective field theory.

The main results of this thesis are based on Ref. [13] and Ref. [14].

# Chapter 2

# AdS/CFT correspondence

In this chapter, we present the basics of the AdS/CFT correspondence briefly.[1]

## 2.1 Basic idea of the AdS/CFT correspondence

The AdS/CFT correspondence relates a gauge theory with a gravity theory. In short, the correspondence states that

$$Z_{\text{gauge}_d} = Z_{\text{AdS}_{d+1}}, \tag{2.1}$$

where $Z_{\text{gauge}_d}$ is a partition function of a $d$-dimensional gauge theory and $Z_{\text{AdS}_{d+1}}$ is a partition function of a $(d+1)$-dimensional gravity theory in an asymptotically anti-de Sitter geometry. The most famous example is the correspondence between 4-dim. $\mathcal{N} = 4$ SU($N$) super Yang-Mills theory and Type IIB supergravity theory on $\text{AdS}_5 \times \text{S}^5$. $\mathcal{N}$ is the number of the supersymmetry and $N$ is the number of color. Many other variations of the correspondence have also been proposed. The idea of the AdS/CFT correspondence was partly motivated by the analogy between the large-$N$ gauge theory and the weakly-coupled string theory. In the large-$N$ gauge theory, the partition function can be written in terms of the bubble diagrams, which is formally expressed as

$$\ln Z_{\text{gauge}} = \sum_{h=0}^{\infty} N^{\chi} f_h(\lambda), \tag{2.2}$$

where $h$ is the genus of the bubble diagrams and $\chi$ is the Euler characteristic which is given by $\chi = 2 - 2h$. $f_h$ is a function of the 't Hooft coupling $\lambda$ at given $h$ which is independent of $N$. Since the $N$-dependence is determined by $\chi$, the leading contribution is given by the planer diagrams: $f_0(\lambda)$. On the other hand, the partition function of the superstring theory can be expressed by

$$\ln Z_{\text{string}} = \sum_{h}^{\infty} g_s^{-\chi} \tilde{f}_h(l_s), \tag{2.3}$$

[1] For references, see [17, 18], for example.

where $g_s$ is the string coupling. $\tilde{f}_h$ is a contribution of the bubble diagrams which is independent of $g_s$ but depends on the string length $l_s$ at given $h$. By comparing these expressions, we may expect the following correspondence:

$$Z_{\text{gauge}} = Z_{\text{string}} \tag{2.4}$$

with

$$g_s \propto \frac{1}{N}, \quad l_s \leftrightarrow \lambda. \tag{2.5}$$

The latter formula in (2.5) means $l_s$ can be written as a function of $\lambda$, *vice versa*. The low-energy effective theory of the superstring theory is a 10-dim. supergravity. This implies that the partition of a gauge theory may be given by a partition function of a supergravity. This idea is made precise by the AdS/CFT correspondence [2–4].

Practically, we replace $Z_{\text{string}}$ with $\exp(-S_{\text{grav}})$ by saddle point approximation, since the exact partition function of the string theory is not known. In the Euclidean formalism, the relationship is expressed by

$$\left\langle \exp\left( \int \mathrm{d}^d x \mathcal{O} \phi_{(0)} \right) \right\rangle = \exp\left(-\bar{S}_{\text{grav}}\right)\big|_{\tilde{\phi}(z=0,x)=\phi_{(0)}(x)}. \tag{2.6}$$

In this expression, $\phi_{(0)}(x)$ denotes the external source for the operator $\mathcal{O}$. In the right-hand side, $\bar{S}_{\text{grav}}$ is the on-shell action for the gravity theory with an asymptotically AdS geometry. We denoted $z$ as the AdS coordinate of the geometry and $z = 0$ is the AdS boundary. $\tilde{\phi}(z, x)$ is the field in the gravity theory corresponding to $\mathcal{O}$ in the gauge theory. This relationship is referred to as *Gubser-Klebanov-Polyakov/Witten relation* [3, 4].

We will consider Type IIB supergravity on $\mathrm{AdS}_5 \times \mathrm{S}^5$ geometry in the right hand side of (2.6). The gravity action (2.13) is proportional to a prefactor $1/2\kappa_{10}^2$. Making the prefactor dimensionless by using the length scale $L$ of the geometry, we obtain

$$\frac{L^8}{2\kappa_{10}^2} = \frac{(4\pi g_s N l_s^4)^2}{(2\pi)^7 g_s^2 l_s^8} \propto N^2. \tag{2.7}$$

The relationship between $L$ and $g_s N l_s^4$ will be given in (2.18). Therefore, the saddle point approximation is valid for large $N$.

## 2.2 D-branes

A D-brane[19] is a solitonic object in the string theory. It is understood as a hyper-surface where endpoints of open strings can be attached. D-branes play crucial roles in the string theory as well as in the AdS/CFT correspondence. In this section, we briefly review the properties of a D-brane.

### 2.2.1 Effective action

In the string theory, the action for a fundamental string is given by the following Nambu-Goto action:

$$S_{\rm NG} = -\frac{1}{2\pi\alpha'}\int {\rm d}^2\sigma\sqrt{-(\dot{X})^2(X')^2 + (\dot{X}\cdot X')^2}, \tag{2.8}$$

where $\sigma^i = (\tau, \sigma)$ are the worldsheet coordinates. $\dot{X}$ and $X'$ denote $\partial_\tau X(\tau,\sigma)$ and $\partial_\sigma X(\tau,\sigma)$, respectively. $1/(2\pi\alpha')$ gives the string tension and it is related to the string scale $l_s$ by $\alpha' = l_s^2$. In analogy with a fundamental string, the bosonic part of the action for a D$p$-brane is given by the following Dirac-Born-Infeld action.

$$\begin{aligned} S_{{\rm D}p} = &-\tau_p\int {\rm d}^{p+1}\xi e^{-\phi}\sqrt{-\det(g_{ab} + B_{ab} + (2\pi\alpha')F_{ab})} \\ &+ \mu_p\int \sum_q C_{(q)}\wedge e^{B+(2\pi\alpha')F}, \end{aligned} \tag{2.9}$$

where $\tau_p$ is the tension of the D$p$-brane and $\mu_p$ is the R-R charge of the D$p$-brane. These are determined as

$$\tau_p = (2\pi)^{-p}{\alpha'}^{-(p+1)/2}, \quad \mu_p = \frac{\tau_p}{g_s}. \tag{2.10}$$

$\xi^a$ are $(p+1)$-dimensional worldvolume coordinates. $g_{ab}$ is the induced metric of the spacetime metric. It is related to the 10-dimensional spacetime metric $g_{MN}$ by

$$g_{ab} = \frac{\partial X^M}{\partial\xi^a}\frac{\partial X^N}{\partial\xi^b}g_{MN}, \tag{2.11}$$

where $X^M$ are 10-dimensional spacetime coordinates. $B_{ab}$ is the induced Kalb-Ramond field which is given by $B_{ab} = B_{MN}\partial_a X^M\partial_b X^N$, where $B_{MN}$ is the Kalb-Ramond field lying on the 10-dimensional spacetime. $F_{ab} = \partial_a A_b - \partial_b A_a$ is the field strength of the gauge field $A_a$ on the D$p$-brane. The second term in (2.9) is called Wess-Zumino term. The summation picks only the appropriate volume-forms in the series expansion of the exponential term. The Wess-Zumino term gives the coupling term between the D$p$-brane and the R-R $(p+1)$-form. This reflects that a D$p$-brane is a $(p+1)$-dimensional R-R charged object.

### 2.2.2 D-branes in supergravity

The low-energy effective theory of the superstring theory is given by the supergravity. Here, we consider the low-energy effective theories of two string theories called Type IIA superstring theory and Type IIB superstring theory. They are referred to as Type IIA supergravity and Type IIB supergravity, respectively.

The bosonic part of the action of Type IIA supergravity is given by

$$S_{\rm IIA} = \frac{1}{2\kappa_{10}^2}\int {\rm d}^{10}X\Big[\sqrt{-g}e^{-2\phi}\left(R + 4(\partial\phi)^2 - \frac{1}{2}\frac{|H_{(3)}|^2}{3!}\right) \\ -\sqrt{-g}\left(\frac{1}{2}\frac{|F_{(2)}|^2}{2!} + \frac{1}{2}\frac{|\tilde{F}_{(4)}|^2}{4!}\right)\Big] - \frac{1}{4}\int B\wedge F_{(4)}\wedge F_{(4)}, \tag{2.12}$$

where $\tilde{F}_{(4)} = F_{(4)} - C_{(1)}\wedge F_{(3)}$, $F_{(p+1)} = {\rm d}C_{(p)}$ and $H_{(3)} = {\rm d}B_{(2)}$. $C_{(p)}$ are R-R $p$-form fields and $B_{(2)}$ is Kalb-Ramond 2-form field. The bosonic part of the action of Type IIB supergravity is given by

$$S_{\rm IIB} = \frac{1}{2\tilde{\kappa}_{10}^2}\int {\rm d}^{10}X\Big[\sqrt{-g}e^{-2\phi}\left(R + 4(\partial\phi)^2 - \frac{1}{2}\frac{|H_{(3)}|^2}{3!}\right) \\ -\sqrt{-g}\left(\frac{1}{2}|F_{(1)}|^2 + \frac{1}{2}\frac{|\tilde{F}_{(3)}|^2}{3!} + \frac{1}{4}\frac{|\tilde{F}_{(5)}|^2}{5!}\right)\Big] \\ -\frac{1}{2}\int C_{(4)}\wedge H_{(3)}\wedge F_{(3)}, \tag{2.13}$$

where $\tilde{F}_{(3)} = F_{(3)} - C_{(0)}\wedge H_{(3)}$ and $\tilde{F}_{(5)} = F_{(5)} - \frac{1}{2}C_{(2)}\wedge H_{(3)} + \frac{1}{2}B_{(2)}\wedge F_{(3)}$. In addition, the self-dual constraint is imposed for the Type IIB supergravity:

$$\star\,\tilde{F}_{(5)} = \tilde{F}_{(5)}. \tag{2.14}$$

$\kappa_{10}$ is related to the 10-dimensional Newton constant $G_{10}$ by $\kappa_{10} = \sqrt{8\pi G_{10}}$. $\tilde{\kappa}_{10} = g_s^{-1}\kappa_{10}$ is the 10-dimensional gravitational. These constants are given by

$$2\kappa_{10}^2 = 2\tilde{\kappa}_{10}^2 g_s^2 = (2\pi)^7\alpha'^4 g_s^2. \tag{2.15}$$

In Type IIB supergravity and Type IIA supergravity, there are solutions corresponding to D$p$-branes. The solutions are called black $p$-brane solutions. These solutions have an isometry of ${\rm ISO}(1,p)\times{\rm SO}(p-1)$ and are explicitly given by

$$\begin{aligned} {\rm d}s^2 =& H_p(r)^{-1/2}\eta_{\mu\nu}{\rm d}x^\mu{\rm d}x^\nu + H_p(r)^{1/2}{\rm d}w^i{\rm d}w^i, && \text{(2.16a)}\\ e^\phi =& g_s H_p(r)^{(3-p)/4}, && \text{(2.16b)}\\ C_{(p+1)} =& \left(H_p(r)^{-1} - 1\right){\rm d}x^0\wedge{\rm d}x^1\wedge\cdots\wedge{\rm d}x^p, && \text{(2.16c)}\\ B =& 0, && \text{(2.16d)} \end{aligned}$$

where $H_p(r) = 1 + (L_p/r)^{7-p}$ and $r^2 = \sum_i {w^i}^2$. $x^\mu$ are the $(p+1)$-dimensional D$p$-brane's worldvolume coordinates. $w^i$ are the $(9-p)$ transverse directions. For Type IIA supergracity, $p$ is even, whereas $p$ is odd for Type IIB supergravity. The black $p$-brane geometries are asymptotically flat.

Let us consider a solution that corresponds to $N$ coincident D3-branes. The number of the D3-branes can be calculated by integrating the R-R flux on a

surface surrounding the D3-brane. This is expressed as

$$N\mu_3 = \frac{1}{2\kappa_{10}^2}\int_{\mathrm{S}^5} \star F_{(5)}. \tag{2.17}$$

For D3-branes, the 5-form flux is given by $\star F_{(5)} = 4L^4(\epsilon(\mathrm{S}^5) + \star\epsilon(\mathrm{S}^5))$ where $\epsilon(\mathrm{S}^5)$ is the volume form of the 5-sphere. By using $\mathrm{Vol}(\mathrm{S}^5) = \pi^3$, we obtain

$$4\pi g_s N = \frac{L^4}{\alpha'^2}. \tag{2.18}$$

### 2.2.3 AdS/CFT correspondence from D3-brane

The D3-brane is a $(3+1)$-dimensional object whose worldvolume theory is a (3+1)-dim. Yang-Mills theory in the low-energy limit. We set $B_{ab} = C_{(p)} = 0$ for simplicity. The fluctuations of the D3-brane in the 6 transverse directions are realized as 6 scalar fields in the worldvolume theory. We consider flat spacetime with constant dilaton $e^{\phi} = g_s$. In a static gauge $\xi^{\mu} = (t, x, y, z)$, the induced metric is written as

$$g_{\mu\nu} = \eta_{\mu\nu} + \partial_\mu X^I \partial_\nu X^J \delta_{IJ}, \tag{2.19}$$

where $\mu, \nu = 0, 1, 2, 3$ are indices for the worldvolume directions and $I, J = 4, 5, 6, 7, 8, 9$ denotes indices for the transverse directions. By setting $\Phi^I = X^I/(2\pi\alpha')$, the DBI action of D3-brane is written as

$$S_{\mathrm{D3}} = -\frac{\tau_3}{g_s}\int \mathrm{d}x^4 \sqrt{-\det(\eta_{\mu\nu} + (2\pi\alpha')F_{\mu\nu} + (2\pi\alpha')^2\partial_\mu\Phi^I\partial_\nu\Phi^I)}. \tag{2.20}$$

We take summation over $I$ from 4 to 9. If we expand the expression in $\alpha'$, we have

$$S_{\mathrm{D3}} = -\frac{\tau_3}{g_s}\int \mathrm{d}^4x \left[\frac{(2\pi\alpha')^2}{4}F_{\mu\nu}F^{\mu\nu} + \frac{(2\pi\alpha')^2}{2}\partial_\mu\Phi^I\partial^\mu\Phi^I + \mathcal{O}\Big(\alpha'^4\Big)\right] \tag{2.21}$$

We omitted the constant term. This is equal to the bosonic part of the action for $\mathcal{N} = 4$ supersymmetric U(1) Yang-Mills theory. So far, we have discussed for the case of a single D3-brane. In the case of $N$ coincident D3-branes, the scalars and gauge fields are generalized to the adjoint representation of U($N$) gauge theory with: $\Phi^I = \Phi^{I\alpha}T_\alpha,\ A_\mu = A_\mu^\alpha T_\alpha$, where $T_\alpha$ is the generator of the U($N$) group. Moreover, we must replace the partial derivative to the covariant derivative and add some potential term. At the leading order in $\alpha'$, the DBI action for $N$ conincident D3-branes gives

$$\begin{aligned} S_{N\times\mathrm{D3}} = -\frac{\tau_3}{g_s}\int \mathrm{d}^4x\, \mathrm{Tr}\Big[&\frac{(2\pi\alpha')^2}{4}F_{\mu\nu}F^{\mu\nu} \\ &+ \frac{(2\pi\alpha')^2}{2}D_\mu\Phi^I D^\mu\Phi^I - \frac{1}{4}\sum_{I,J}\big[\Phi^I, \Phi^J\big]^2\Big], \end{aligned} \tag{2.22}$$

where the covariant derivative is given by $D_\mu \Phi^I = \partial_\mu \Phi^I + i\big[A_\mu, \Phi^I\big]$, and the field strength is given by $F_{\mu\nu} = \partial_\mu A_\nu - \partial_\nu A_\mu + i[A_\mu, A_\nu]$. This action corresponds to the bosonic part of the action of the $\mathcal{N} = 4$ supersymmetric U($N$) Yang-Mills (SYM) theory. By comparing to the action of the conventional pure Yang-Mills theory

$$S_{\rm YM} = -\int \mathrm{d}^4x \frac{1}{4g_{\rm YM}^2} \,\mathrm{Tr}\, F_{\mu\nu}F^{\mu\nu}, \tag{2.23}$$

we find the Yang-Mills coupling as

$$g_{\rm YM}^2 = \frac{g_s}{\tau_3 (2\pi\alpha')^2} = 2\pi g_s. \tag{2.24}$$

As discussed above, the worldvolume theory of the D3-brane describes $(3+1)$-dimensional $\mathcal{N} = 4$ SYM theory in the low-energy limit. On the other hand, the D3-brane is also expressed as the black 3-brane solution (2.16) in the supergravity theory. The black 3-brane geometry is given by

$$\mathrm{d}s^2 = \left(1 + \frac{L^4}{r^4}\right)^{-\frac{1}{2}} \eta_{\mu\nu}\mathrm{d}x^\mu \mathrm{d}x^\nu + \left(1 + \frac{L^4}{r^4}\right)^{\frac{1}{2}} \left(\mathrm{d}r^2 + r^2 \mathrm{d}\Omega_5^2\right), \tag{2.25}$$

where $\mathrm{d}\Omega_5^2$ is the line element of the unit 5-sphere.

The physical modes on the black 3-brane geometry may contain the physical degrees of freedom of the D3-brane, but they contain the physical degrees of freedom of the peripheral supergravity, as well. Therefore, let us take a limit to extract the information of the physics of the worldvolume theory of D3-brane. In order to focus on the degrees of freedom of the YM theory on the D3-brane, we take a limit $r \ll L$. Then the black-3 brane geometry reduces to $\mathrm{AdS}_5 \times \mathrm{S}^5$:

$$\mathrm{d}s^2 = \frac{r^2}{L^2}\eta_{\mu\nu}\mathrm{d}x^\mu \mathrm{d}x^\nu + \frac{L^2}{r^2}\mathrm{d}r^2 + L^2 \mathrm{d}\Omega_5^2. \tag{2.26}$$

This limit is called as *near horizon limit* or *throat limit*. The geometry has the isometry of $\mathrm{SO}(2,4)_{\mathrm{AdS}_5} \times \mathrm{SO}(6)_{\mathrm{S}^5}$. This corresponds to the symmetry of $\mathcal{N} = 4$ SU($N$) SYM theory: $\mathrm{SO}(2,4)_{\rm CFT} \times \mathrm{SO}(6)_{\rm R}$. It is known that the degrees of freedom of the U(1) part of $\mathrm{U}(N) = \mathrm{U}(1) \times \mathrm{SU}(N)$ are decoupled.[2] The near horizon limit extracts the degrees of freedom of the $\mathcal{N} = 4$ SU($N$) SYM theory from the supergravity theory on the black 3-brane geometry.

We regard the number of the D3-brane as the number of the color $N$ in the SYM theory. We obtain

$$2\pi g_s = \frac{\lambda}{N}, \quad \frac{L^4}{l_s^4} = 2\lambda, \tag{2.27}$$

from (2.24) and (2.18). This agrees with the naive expectation (2.5).

The AdS/CFT correspondence can be generalized to finite temperature cases. This is achieved by replacing the geometry to a black hole geometry. Then, the

[2] In Ref. [20], this is discussed that such a degree of freedom can only enter the AdS/CFT correspondence as a singleton field supported at the AdS boundary.

Hawking temperature is regarded as the temperature of the dual field theory. The black hole geometry called near extremal black $p$-brane is given by

$$\mathrm{d}s^2 = H_p^{-\frac{1}{2}}\left(-f(r)\mathrm{d}t + \mathrm{d}\vec{x}_p^2\right) + H_p^{\frac{1}{2}}\left(\frac{\mathrm{d}r^2}{f(r)} + r^2\mathrm{d}\Omega_{8-p}^2\right), \tag{2.28}$$

where $f(r) = 1 - r_h^{7-p}/r^{7-p}$.[21] $r_h$ is the location of the black hole horizon. Let us take $p = 3$ to consider the D3-brane case. In the near horizon limit, $r \ll L$, the geometry reduces to the Schwarzschild $\mathrm{AdS}_5 \times \mathrm{S}^5$ geometry:

$$\mathrm{d}s^2 = \frac{r^2}{L^2}\left(-f(r)\mathrm{d}t + \mathrm{d}\vec{x}^2\right) + L^2\frac{\mathrm{d}r^2}{r^2 f(r)} + L^2\mathrm{d}\Omega_5^2. \tag{2.29}$$

The location of the black hole horizon is related to the Hawking temperature by $r_h = L^2\pi T$. The symmetry of the geometry is reduced from $\mathrm{ISO}(1,4) \times \mathrm{SO}(6)$ to $\mathrm{SO}(3) \times \mathrm{SO}(6)$.

## 2.3 Wilson loop

In the gauge theory, the Wilson loop is a observable from which one can read the potential energy between quark and anti-quark. The expectation value of the Wilson loop can be also computed from the AdS/CFT corresponding.[22][3] Our goal of this thesis is analyzing the lifetime of a bound state consisting of the charged particle and anti-particle. It is worth studying the potential energy in the framework of the gravity model with $\mathrm{AdS}_5$ geometry.

The Wilson loop is given by

$$W(C) = \mathcal{P}\exp\left(i\oint_C A_\mu \mathrm{d}x^\mu\right), \tag{2.30}$$

where $\mathcal{P}$ denotes the path-order operation. The Wilson loop depends on a contour $C$. The expectation value of the Wilson line is related to the partition function $Z_\delta$ of the gauge theory with a test particle:

$$\langle W(C)\rangle = \int \mathcal{D}\phi \exp\left[iS_{\text{gauge}} + i\oint_C A_\mu \mathrm{d}x^\mu\right] = \frac{Z_\delta}{Z_0}, \tag{2.31}$$

where $Z_0$ is vacuum partition function of the gauge theory. We choose $C$ as rectangle path which has a time interval $\Delta t$ and a separation $\Delta x$. (See Fig. 2.1.) In a limit of $\Delta t \to \infty$, the contribution of the Wilson loop is equivalent to the one where the particle and the anti-particle reside separated by $\Delta x$ at rest. Then, the partition function is written as

$$Z_\delta(\Delta x) \propto \exp(-i\Delta t V(\Delta x)), \tag{2.32}$$

where $V(\Delta x)$ is the potential energy between the charged particle and the anti-particle at rest.

[3] For reviews see [17].

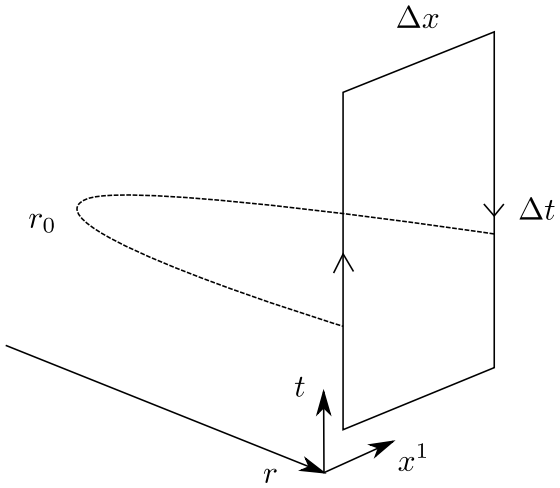


Figure 2.1: Schematic picture of the Wilson loop in the AdS/CFT correspondence. The rectangle shows the contour we consider here in the field theory. The dashed line shows the embedding configuration of the test string in a some time slice.

In the AdS/CFT correspondence, a probe string play a role of the test particle. Two endpoints of the probe string at the AdS boundary correspond to the charged particle and the anti-particle. The Wilson loop can be evaluated from the on-shell value of the probe string. We consider the $AdS_5$ geometry (2.26). In this computation, the 5-sphere part does not contribute. The action of the probe string is given by the Nambu-Goto action (2.8). We choose the static gauge for the worldsheet coordinates: $\tau = t$ and $\sigma = r$. Assuming $\vec{x} = (x(r), 0, 0)$, the action is written as

$$S_{\rm NG} = -\frac{1}{2\pi\alpha'}\int {\rm d}t{\rm d}r\sqrt{1+\frac{r^4}{L^4}x'(r)^2}. \tag{2.33}$$

The constant of motion for $x(r)$ is given by

$$\frac{r_0^2}{L^2} = \frac{\frac{r^4}{L^4}x'(r)}{\sqrt{1+\frac{r^4}{L^4}x'(t)^2}}, \tag{2.34}$$

where $r = r_0$ is a turning point which satisfies $x'(r_0) = \infty$. By solving (2.34) for $x'(r)$ and integrating it, we obtain the solution as

$$x(r) = \int_{r_0}^{r}\frac{L^4}{r^4}\frac{{\rm d}r}{r^4/r_0^4-1}. \tag{2.35}$$

At the boundary, $x(\infty)$ is regarded as $\Delta x/2$ where $\Delta x$ is a separation of each

endpoint of the probe string. This is related to $r_0$ by

$$\frac{\Delta x}{2} = \frac{L^2}{r_0}\int_1^\infty \frac{\mathrm{d}\rho}{\rho^2\sqrt{\rho^4-1}} = \frac{\sqrt{2}\pi^{3/2}}{\Gamma(1/4)^2}\frac{L^2}{r_0}. \tag{2.36}$$

The potential energy is given by the following expression.

$$V(\Delta x) = E - E_0, \tag{2.37}$$

where

$$E = -2L = \frac{2}{2\pi\alpha'}r_0\int_1^\infty \frac{\rho^2\mathrm{d}\rho}{\sqrt{\rho^4-1}}, \tag{2.38a}$$

$$E_0 = -2L_0 = \frac{2}{2\pi\alpha'}r_0\int_0^\infty \mathrm{d}\rho. \tag{2.38b}$$

The energy $E$ is related to the on-shell Lagrangian $L$ from the discussion above. The factor of 2 appears because the solution represents half of the test string. Notice that, this quantity is not finite since the test string has infinite mass. So we subtracted the contribution of the infinite mass, $E_0$, where $L_0$ is an on-shell Lagrangian with a straight string hanging from $r = \infty$ to $r = 0$. Then, the potential energy is written as

$$V(\Delta x) = -\frac{4\pi^2}{\Gamma(1/4)^4}\frac{\sqrt{2\lambda}}{\Delta x}. \tag{2.39}$$

This is a Coulomb type potential energy. This result is consistent with the $\mathcal{N}=4$ SYM theory which has no scale.

We can also compute the potential energy at finite temperatures.[23] We consider the background spacetime as the Schwarzschild $AdS_5$ geometry (2.29). Then, the action is written as

$$S_{\mathrm{NG}} = -\frac{1}{2\pi\alpha'}\int \mathrm{d}t\mathrm{d}r\sqrt{1+x'(r)^2 f(r)\frac{r^4}{L^4}}. \tag{2.40}$$

The solution of the embedding function is given by

$$x(r) = \int_{r_0}^r \frac{L^2}{r^2}\sqrt{\frac{r_0^4 f(r_0)}{f(r)(r^4 f(r) - r_0^4 f(r_0))}}\mathrm{d}r. \tag{2.41}$$

The separation is given by

$$\Delta x = 2x(\infty) = 2\frac{L^2}{\pi T}\int_{\rho_0}^\infty \frac{1}{\rho^2}\sqrt{\frac{\rho_0^4 f(\rho_0)}{f(\rho)(\rho^4 f(\rho) - \rho_0^4 f(\rho_0))}}\mathrm{d}\rho, \tag{2.42}$$

where $\rho_0 = r_0/r_h$. By substituting the solution into the action, the potential energy is given by

$$V(\Delta x) = \sqrt{2\lambda}\frac{T}{L^2}\left[\int_{\rho_0}^\infty \left(\sqrt{\frac{\rho^4 f(\rho)}{\rho^4 f(\rho) - \rho_0^4 f(\rho_0)}} - 1\right)\mathrm{d}\rho - (\rho_0 - 1)\right], \tag{2.43}$$

where $\rho_0$ is related to $\Delta x$ by (2.42). For large $\Delta x$, the test string hanging from the boundary can split into two strings which has one of the endpoints at the black hole horizon. In this case, the potential energy is given by $V(\Delta x) = 0$.

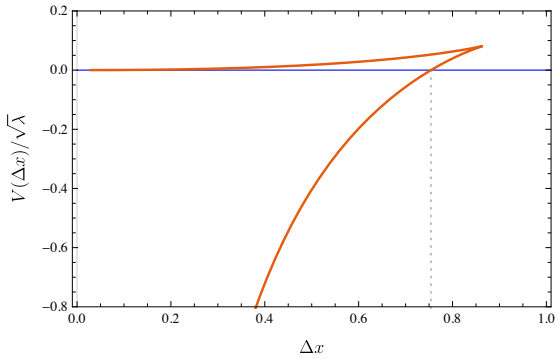


Figure 2.2: Potential energy as a function of the separation at $T = 1/\pi$. The red line corresponds to the solution of the string without touching to the black hole horizon. The blue line corresponds to the individual two strings. The dotted line denotes a crossing point at $\Delta x = 0.75407$. The branch of the lower red line is thermodynamically stable for $\Delta x < 0.75407$, otherwise the blue line is stable.

Fig. 2.2 shows the numerical result of $V(\Delta x)$ verses $\Delta x$ at a finite temperature. Here, we set $T = 1/\pi$. The red line corresponds to the solution that the string does not reach the black hole horizon that gives the potential energy (2.43). The blue line corresponds to the solution given by two individual strings. At finite temperatures, $V(\Delta x)$ is a multivalued function of $\Delta x$. The lower branches are always stable from the thermodynamic analysis. There is a crossing point of the red line and the blue line at $\Delta x = 0.75407$. The phase transition occurs at this point. The crossing point corresponds to the Debye length of the system at the finite temperature.

# Chapter 3

# D3-D7 model

As we have seen in the previous chapter, we can find the correspondence between gravity theory with $AdS_5$ geometry and $d = 4$ SYM theory, by considering D3-branes. D3-branes only represent, however, pure SYM theory without matter fields. In order to consider the degrees of freedom of matter fields such as quarks, one can use a method known as Karch-Katz model [10]. In this model, additional branes represent the degrees of freedom of the matter fields. Particularly, the model with a combination of D3-branes and D7-branes which is called *D3-D7 model*, represents the $\mathcal{N} = 4$ SYM theory and the $\mathcal{N} = 2$ hypermultiplet in the $d = 3 + 1$ dimensional spacetime. In this section, we briefly review the D3-D7 model. The D3-D7 model also represents electric conductor, called as a *holographic conductor* model. In this model, the system exhibits a negative differential conductivity for small range of the parameters. Our goal of this thesis is clarifying the mechanism of this negative differential conductivity.

D-branes is a hyper-surface on which the endpoints of the open strings can be attached. A D$p$-brane enforces Neumann conditions along its $(p+1)$ worldvolume directions, otherwise Dirichlet conditions for the open strings. A combination of D$p$-branes and D$q$-branes provides mixed boundary condition for strings. The D-branes configuration of the D3-D7 model is shown in Table 3.1. The D3-D7 model provides 4 Neumann-Dirichlet directions. The D3-brane's worldvolume coordinates correspond to the 4-dim. Minkowski coordinates of the dual field theory. The D7-brane's worldvolume also shares this 4-dim. coordinates. Since the D7 brane has two transverse directions, there are two scalar fields on the D7-brane. The rotational symmetry in the compact direction corresponds to the internal symmetry called R-symmetry in the dual field theory. Particularly,

| | $x^0$ | $x^1$ | $x^2$ | $x^3$ | $w^1$ | $w^2$ | $w^3$ | $w^4$ | $w^5$ | $w^6$ |
|---|---|---|---|---|---|---|---|---|---|---|
| $N_c$ D3 | ✓ | ✓ | ✓ | ✓ | | | | | | |
| $N_f$ D7 | ✓ | ✓ | ✓ | ✓ | ✓ | ✓ | ✓ | ✓ | | |

Table 3.1: Configuration of the D3-D7 model.

the rotational symmetry in the transverse $w^5$-$w^6$ plane is regarded as the $\mathrm{U}(1)_R$ chiral symmetry. The combination of $w^5 + iw^6$ corresponds to the complex scalar field in the dual field theory.

In the gravity side, the scalar fields represent the location of the D7 brane in the 10-dimensional spacetime. This is often called the *embedding*. The embedding function is determined by solving the equation of motion for the scalar fields. The number of the D7-branes gives the number of flaver $N_f$ of the matter fields. However, we set $N_f = 1$ in the following part of the thesis.

## 3.1 Zero temperature

Let us consider the D3-D7 model with massive quarks at zero temperature. We write the background metric of $\mathrm{AdS}_5 \times \mathrm{S}^5$ spacetime (2.26) as

$$\mathrm{d}s^2 = \frac{w^2}{L^2}\eta_{\mu\nu}\mathrm{d}x^\mu \mathrm{d}x^\nu + \frac{L^2}{w^2}\left(\mathrm{d}\rho^2 + \rho^2 \mathrm{d}\Omega_3^2 + \mathrm{d}w_5^2 + \mathrm{d}w_6^2,\right) \tag{3.1}$$

where $w^2 = \rho^2 + w_5^2 + w_6^2$. In a probe limit, we consider the dynamics of the D7-brane in this curved spacetime. The action for the D7-brane is given by the DBI action (2.9). There are two scalar fields and one vector field living on the D7-brane's worldvolume. For simplicity, we set the vector fields to zero. The two scalar fields arising from the two direction which is perpendicular to the D7-brane's worldvolume represent the embedding function of the D7-brane in the 10-dimensional spacetime. We set the worldvolume coordinates of the D7-brane to $\xi^a = (x^\mu, \rho, \Omega_3)$ called static gauge. The two scalar fields are $w_5$ and $w_6$. Assuming $w_5 = w_5(\rho)$ and $w_6 = 0$, the action (2.9) is written as

$$S_{\mathrm{D7}} = -\frac{\tau_7}{g_s}\mathrm{Vol}(\mathrm{S}^3)\int \mathrm{d}^4x \mathrm{d}\rho \rho^3 \sqrt{1 + w_5'(\rho)}, \tag{3.2}$$

where $w_5'(\rho) = \partial_\rho w_5(\rho)$. The equation of motion for $w_5(\rho)$ is given by

$$0 = \frac{\partial}{\partial\rho}\left[\frac{\rho^3}{\sqrt{1 + w_5'(\rho)^2}} w_5'(\rho)\right]. \tag{3.3}$$

Obviously, $w_5 = l_q$ with a constant $l_q$ is a solution of the embedding function. This result is consistent with the fact there is no interaction between D-branes preserving the supersymmetry. The energy of 3-7 string corresponds to the mass of the quark $m_q$. Taking account of the string tension, we obtain the precise relationship:

$$m_q = \frac{l_q}{2\pi\alpha'}. \tag{3.4}$$

### 3.1.1 "Meson" spectrum

At zero temperature and without external fields, the solution of the embedding function is simply given by $w_5 = l_q$. In this case, the analytic solutions of the

perturbation fields and the expression of the mass spectrum of the meson-like bound states have been obtained in Ref. [24]. We reparameterize the perturbation fields as

$$w_5 = l_q + 2\pi\alpha'\varphi, \quad w_6 = 0 + 2\pi\alpha'\chi. \tag{3.5}$$

The relevant part of the Lagrangian density is written as

$$\mathcal{L} \simeq -\frac{\tau_7}{g_s}\sqrt{-\det h_{ab}}\left[1 + \frac{(2\pi\alpha')^2}{2}\frac{L^2}{w^2}h^{cd}\left(\partial_c\chi\partial_d\chi + \partial_c\varphi\partial_d\varphi\right)\right], \tag{3.6}$$

where $h_{ab}$ denotes the induced metric without the perturbation fields and $h^{ab}$ is its inverse matrix. Now, the induced metric is written as

$$h_{ab}\mathrm{d}\xi^a\mathrm{d}\xi^b = \frac{w^2}{L^2}\eta_{\mu\nu}\mathrm{d}x^\mu\mathrm{d}x^\nu + \frac{L^2}{w^2}\left(\mathrm{d}\rho^2 + \rho^2\mathrm{d}\Omega_3^2\right), \tag{3.7}$$

where $w^2$ can be written as $\rho^2 + l_q^2$. The equations of motions for $\chi$ and $\varphi$ are given by the same equation. We write it

$$0 = \partial_a\left[\frac{1}{w^2}\sqrt{-\det h_{ab}}h^{ab}\partial_b\Phi\right] = \partial_a\left[\frac{\rho^3}{w^2}\sqrt{\det\tilde{h}_{ij}}h^{ab}\partial_b\Phi\right], \tag{3.8}$$

where $\tilde{h}_{ij}$ is defined by $\tilde{h}_{ij}\mathrm{d}\xi^i\mathrm{d}\xi^j = \mathrm{d}\Omega_3^2$ for $i,j = 1,2,3$. $\Phi$ denotes $\chi$ or $\varphi$. The equation is expanded as

$$0 = \frac{1}{\rho^3}\partial_\rho(\rho^3\partial_\rho\Phi) + \frac{L^4}{w^2}\Box\Phi + \frac{1}{\rho^2}\nabla^i\nabla_i\Phi, \tag{3.9}$$

where $\Box = \eta^{\mu\nu}\partial_\mu\partial_\nu$ and

$$\nabla^i\nabla_i = \frac{1}{\sqrt{\det\tilde{h}_{ij}}}\partial_i\sqrt{\det\tilde{h}_{ij}}\tilde{h}^{ij}\partial_j \tag{3.10}$$

which is the Laplace-Beltrami operator on $\mathrm{S}^3$. We employ the ansatz:

$$\Phi = \phi(\rho)e^{ik\cdot x}\mathcal{Y}^l(\mathrm{S}^3), \tag{3.11}$$

where $\mathcal{Y}^l(\mathrm{S}^3)$ is the spherical harmonic function on $\mathrm{S}^3$ which gives $\nabla^i\nabla_i\mathcal{Y}^l(\mathrm{S}^3) = -l(l+2)\mathcal{Y}^l(\mathrm{S}^3)$. After some transformations of variables, we obtain the expression as

$$0 = y(1-y)\partial_y^2P(y) + [c - (a+b+1)y]\partial_yP'(y) - abP(y), \tag{3.12}$$

with $a = -\alpha$, $b = -\alpha + l + 1$ and $c = l + 2$. The relationships between new and old variables are

$$\begin{gathered}\phi = \varrho^l(1+\varrho^2)^{-\alpha}P, \quad -\varrho^2 = y, \\ 2\alpha = -1 + \sqrt{1+\bar{M}^2}, \quad \varrho = \rho/l_q, \quad \bar{M}^2 = -k^2L^4/l_q^2.\end{gathered} \tag{3.13}$$

Under the regularity conditions, the solution is given by a hypergeometric function:

$$P(y) = {}_2F_1(a,b;c;y). \tag{3.14}$$

So we write

$$\phi(\rho) = \rho^l(\rho^2 + L^2)^{-\alpha}{}_2F_1(-\alpha, -\alpha + l + 1; l + 2; -\rho^2/L^2). \tag{3.15}$$

In the framework of the AdS/CFT correspondence, the normalizable mode corresponds to a dynamical mode of the field theory. From asymptotic behavior of this function in the vicinity of $\rho = \infty$, the solution that represents the normalizable modes is given by

$$\phi(\rho) = \frac{\rho^l}{(\rho^2 + l_q^2)^{n+l+1}}{}_2F_1(-(n + l + 1), -n; l + 2; -\rho^2/L^2), \tag{3.16}$$

where $n = -\alpha+l+1$ is restricted for $n = 0, 1, 2\cdots$. Therefore the mass spectrum $M = \sqrt{-k^2}$ is given by

$$M(n, l) = \frac{2l_q}{L^2}\sqrt{(n + l + 1)(n + l + 2)} = 2\pi m_q\sqrt{\frac{(n + l + 1)(n + l + 2)}{2g^2_{\rm YM}N_c}}. \tag{3.17}$$

Here we use $2g_{\rm YM^2}N_c = L^4/\alpha'^2$. The mass of the lightest bound state is given by

$$M(0, 0) = 2\sqrt{2}\frac{l_q}{L^2} = \frac{2\pi m_q}{\sqrt{g^2_{\rm YM}N_c}} = \frac{2\pi m_q}{\sqrt{\lambda}}. \tag{3.18}$$

This expression is also valid for the vector bound state corresponding to $A_a(\xi)$ on the brane.

## 3.2 Finite temperatures

At finite temperatures, we consider Schwarzschild-AdS$_5 \times$ S$^5$ geometry (2.29) as the background spacetime. We consider the following coordinate transformation:

$$\tilde{w} = \frac{1}{r_h}\sqrt{r^2 + \sqrt{r^4 - r_h^4}}. \tag{3.19}$$

In this coordinate, the metric is written as

$$\mathrm{d}s^2_{10} = \frac{1}{2}\left(\frac{r_h\tilde{w}}{L}\right)^2\left[-\frac{f^2(\tilde{w})}{\tilde{f}(\tilde{w})}\mathrm{d}t^2 + \tilde{f}(\tilde{w})\mathrm{d}\vec{x}^2\right] + \frac{L^2}{\tilde{w}^2}\left[\mathrm{d}\tilde{w}^2 + \tilde{w}^2\mathrm{d}\Omega_5^2\right], \tag{3.20}$$

where $f(\tilde{w}) = 1 - \tilde{w}^{-4}$ and $\tilde{f}(\tilde{w}) = 1 + \tilde{w}^{-4}$. Now, $\tilde{w}$ gives the radius of the 5-sphere. $L$ is the AdS radius. This is a finite temperature version of (3.1). In the vicinity of the AdS boundary $\tilde{w} = +\infty$, the geometry reduces to AdS$_5 \times$ S$^5$. The black hole horizon is located at $\tilde{w} = 1$. $r_h$ is related to the Hawking temperature by $T = r_h/(\pi L^2)$. $\mathrm{d}\Omega_5$ is the line element of a unit 5-sphere which can be decomposed as

$$\mathrm{d}\Omega_5^2 = \mathrm{d}\theta^2 + \sin^2\theta\mathrm{d}\Omega_3^2 + \cos^2\theta\mathrm{d}\psi^2, \tag{3.21}$$

where $0 \leq \theta \leq \pi/2$ and $0 \leq \psi < 2\pi$ are the $S^2$ coordinates. In the static gauge $\xi^a = (t, \vec{x}, \tilde{w}, \Omega_3)$, the induced metric is written as

$$\begin{aligned} \mathrm{d}s^2 = \frac{1}{2}\left(\frac{r_h \tilde{w}}{L}\right)^2 \left[-\frac{f^2(\tilde{w})}{\tilde{f}(\tilde{w})}\mathrm{d}t^2 + \tilde{f}\mathrm{d}\vec{x}^2\right] \\ + \left(\frac{L^2}{\tilde{w}^2} + \frac{L^2\chi'(\tilde{w})^2}{1-\chi(\tilde{w})^2}\right)\mathrm{d}\tilde{w}^2 + L^2(1-\chi^2)\mathrm{d}\Omega_5^2, \end{aligned} \tag{3.22}$$

where $\chi(\tilde{w}) \equiv \cos\theta(\tilde{w})$ and we set $\psi = 0$ by virtue of the symmetry. $\chi'(\tilde{w})$ denotes $\partial_{\tilde{w}}\chi$. The embedding function is obtained by solving the equation of motion for $\chi(\tilde{w})$. There are no analytic solution known except for a trivial embedding: $\chi(\tilde{w}) = 0$. The trivial embedding corresponds to the system with vanishing quark mass and preserving the chiral symmetry.

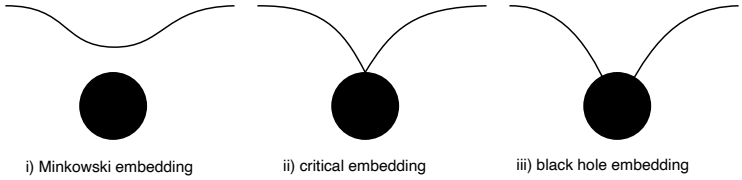


Figure 3.1: Sketch of the three types of the embedding in the D3-D7 model at finite temperature.

In [25], it has been found that the embeddings of the probe brane are classified into three types. Fig. 3.1 shows the typical shapes of the three types of the embedding. When the probe brane does not touch the black hole horizon, the configuration is classified as a i) Minkowski embedding. Otherwise, the configuration is classified as a iii) black hole embedding when the probe brane touches the black hole horizon. Exceptionally, if the probe brane touches a point on the black hole horizon, the configuration is classified as a ii) critical embedding. However, we do not consider this case because the critical embedding is only observed under an extreme situation of the probe brane.

### 3.2.1 Quasi-normal modes

We briefly review the mass spectrum of the charged vector particle at finite temperatures.[1] We consider the background configuration as $\chi(\tilde{w}) = 0$ corresponding to the massless case. This is classified as the black hole embedding. In this configuration, the complex mass spectrum can be calculated as a quasinormal mode (QNM) spectrum in the gravity side. The relevant term of the DBI action is given by

$$S \simeq -\frac{(2\pi l_s^2)^2}{4} N_f \int \mathrm{d}^8\xi \sqrt{-\det h_{ab}}\, h^{cd} h^{ef} F_{fc} F_{de} \tag{3.23}$$

[1] See [26] for more detailed discussions. The mass spectrum of the scalar field has been studied in Ref. [27].

The equation of motion is given by the Maxwell equation on the curved spacetime:

$$0 = \partial_b \left[ \sqrt{-\det h_{ab}} h^{ac} F_{cd} h^{db} \right]. \tag{3.24}$$

We employ the ansatz as

$$A_\mu = \sum_l \mathcal{Y}^l(\mathrm{S}^3) A^l_\mu(\tilde{w}, t), \tag{3.25}$$

for $\mu = t, x, y, z$. For $E_l \equiv \omega A^l_i$, the equation of motion is written as

$$\begin{aligned} E_l''(\tilde{w}) + \left[ \frac{4f'(\tilde{w})}{\tilde{f}f} + \frac{f}{\tilde{f}^2} \frac{\sqrt{1-\chi^2+\tilde{w}^2\chi'(\tilde{w})^2}}{\tilde{w}^3(1-\chi^2)^2} \partial_{\tilde{w}} \left( \frac{\tilde{f}^2\tilde{w}^3(1-\chi^2)^2}{f\sqrt{1-\chi^2+\tilde{w}^2\chi'(\tilde{w})^2}} \right) \right] E_l'(\tilde{w}) \\ + \frac{1-\chi^2+\tilde{w}^2\chi'(\tilde{w})^2}{\tilde{w}^2(1-\chi^2)^2} \left[ \frac{8(1-\chi^2)\tilde{f}}{\tilde{w}^2 f^2} \mathfrak{w}^2 - l(l+2) \right] E_l(\tilde{w}) = 0, \end{aligned} \tag{3.26}$$

where $\mathfrak{w} = \omega/(2\pi T)$. In the massless case, $\chi$ is set to zero. Making change of variables $\bar{x} = 1 - 2\tilde{w}^2/\tilde{f}(\tilde{w}) = 1 - 2\tilde{w}^2/(1+\tilde{w}^4)$, the equation is written as

$$E_l''(\bar{x}) + \frac{f'(\bar{x})}{f} E_l'(\bar{x}) + \left[ \frac{\mathfrak{w}^2}{(1-\bar{x})f^2} - \frac{l(l-2)}{4(1-\bar{x})^2 f} \right] E_l(\bar{x}) = 0. \tag{3.27}$$

By performing Frobenius expansion at $\bar{x} = 0$, we have two distinct solutions:

$$E_l(\bar{x}) = \bar{x}^{-i\mathfrak{w}/2} E_l^{(-)}(\bar{x}) + \bar{x}^{i\mathfrak{w}/2} E_l^{(+)}(\bar{x}), \tag{3.28}$$

where $E_l^{(\pm)}(\bar{x})$ are the regular function at $\bar{x} = 0$. It is known that the *ingoing-wave solution* where the perturbation falls into the horizon gives physical results. In this case the solution expressed by the first term corresponds to the ingoing-wave solution, so we set $E_l^{(+)} = 0$. We choose the ingoing-wave solution which is given by

$$E_l(\bar{x}) = \bar{x}^{-i\mathfrak{w}/2} (2-\bar{x})^{-\mathfrak{w}/2} F(\bar{x}), \tag{3.29}$$

where the regular function $F$ is written as

$$F(\bar{x}) = (1-\bar{x})^{\frac{(1+i)\mathfrak{w}}{2}} {}_2F_1 \left( 1 + \frac{l}{2} - \frac{(1+i)\mathfrak{w}}{2}, -\frac{l}{2} - \frac{(1+i)\mathfrak{w}}{2}; 1 - i\mathfrak{w}; \frac{\bar{x}}{2(\bar{x}-1)} \right). \tag{3.30}$$

The AdS boundary is located at $\bar{x} = 1$. The normalizable condition requests $F(1) = 0$. The leading term of $F$ in the vicinity of $\bar{x} = 1$ is given by

$$F(x) \approx 2^{a+\alpha}(1-\bar{x})^b \frac{\Gamma(a-b)\Gamma(c)}{\Gamma(c-b-\alpha)\Gamma(a+\alpha)}, \tag{3.31}$$

where $\alpha = -(1+i)\mathfrak{w}/2$, $a = 1 + l/2$, $b = -l/2$ and $c = 1 - i\mathfrak{w}$. The only way to make this term vanishing is to make the gamma functions in the denominator diverge. Gamma functions have poles at zero and negative integer values,

therefore the normalizable condition is satisfied by $c-a-\alpha=-n,\ b+\alpha=-n$, for $n=0,1,2,3,\cdots$. This condition gives the complex mass spectrum which is written as

$$\mathfrak{w}=\pm\left(n+1+\frac{l}{2}\right)(1\pm i). \tag{3.32}$$

This corresponds to the location of the poles of the two-point function of the dual operator in the boundary theory. Writing $\omega=\mathcal{E}-i\Gamma/2$, $\mathcal{E}$ and $\Gamma$ are understood as the energy (or mass) and the decay width of the quasi-particle, respectively. Notice that you can apply quasi-particle picture only when $\Gamma<\mathcal{E}$. In the present result, we should call it as resonance states rather than quasi-particle since $\Gamma$ is equal to $\mathcal{E}$ for all $n$ and $l$.

## 3.3 Holographic conductor

One finds that the system in the D3-D7 model has a finite electric conductivity.[11] In general, a model of AdS/CFT correspondence which shows electric conductivity is called as a *holographic conductor*. Since the normalizable mode of the U(1) gauge field $A_\mu$ on the D7-brane corresponds to the expectation value of the $\mathrm{U(1)_V}$ current operator in the dual field theory, we can compute the electric conductivity of the D3-D7 model. This system also shows a negative differential conductivity (NDC) [5], which has been widely observed in strongly correlated electron systems. In this section, We briefly review how the NDC is realized in the D3-D7 model.

In this model, the system is an insulator at low temperature, whereas we have finite conductivity at high temperatures. The heat bath is realized as the 5-dimensional asymptotically AdS-Schwarzschild black hole geometry times $\mathrm{S}^5$ given at (3.20). By transforming the coordinate: $\tilde{w}=z_h/z$ with $r_h=\sqrt{2}/z_h$, we write the spacetime metric as [2]

$$\mathrm{d}s_{10}^2=g_{MN}\mathrm{d}X^M\mathrm{d}X^N=\frac{1}{z^2}\left[-\frac{f(z)^2}{\tilde{f}(z)}\mathrm{d}t^2+\tilde{f}(z)\mathrm{d}\vec{x}^2\right]+\frac{\mathrm{d}z^2}{z^2}+\mathrm{d}\Omega_5^2, \tag{3.33}$$

where

$$f(z)=1-z^4/z_h^4,\quad \tilde{f}(z)=1+z^4/z_h^4. \tag{3.34}$$

We have set the AdS radius $L$ to 1. $z=z_h$ is the location of the black hole horizon. The Hawking temperature is given by $T=\frac{\sqrt{2}}{\pi z_h}$. $\mathrm{d}\Omega_5$ denotes the line element of the unit 5-sphere.

The system of charged particles is given as an D7-brane whose action is (2.9)[3]:

$$S_{\mathrm{D7}}=-\frac{\tau_7}{g_s}\int\mathrm{d}^8\xi\sqrt{-\det(g_{ab}+F_{ab})},\quad g_{ab}=g_{MN}\frac{\partial X^M}{\partial\xi^a}\frac{\partial X^N}{\partial\xi^b}, \tag{3.35}$$

[2] We write $M,N$ as indices of the spacetime coordinates $X^N$ which run from 0 to 9.

[3] We set $(2\pi\alpha')=1$. $a,b$ are indices of the worldvolume coordinates of the D7-brane $\xi^a$ which run from 0 to 7.

where $\tau_7$ is the tension of the D7-brane, $\xi^a$ are the worldvolume coordinates, $g_{ab}$ is the induced metric and $F_{ab} = \partial_a A_b - \partial_b A_a$ is the field strength. In the D3-D7 model, the D7-brane is wrapped on the $S^3$ part of the $S^5$. The metric of $S^5$ part can be written as (3.21). We employ a static gauge $\xi^a = (t, \vec{x}, z, \Omega^3)$, then $\theta(\xi)$ and $\psi(\xi)$ are dynamical fields. We assume that $\theta(\xi)$ depends only on $z$, and $\psi(\xi)$ is set to zero by virtue of the symmetry. The induced metric is written as

$$g_{ab}\mathrm{d}\xi^a\mathrm{d}\xi^b = \frac{1}{z^2}\left[-\frac{f(z)^2}{\tilde{f}(z)}\mathrm{d}t^2 + \tilde{f}(z)\mathrm{d}\vec{x}^2\right] + \left(\frac{1}{z^2} + \theta'(z)^2\right)\mathrm{d}z^2 + \cos^2\theta\mathrm{d}\Omega_3^2. \tag{3.36}$$

From this metric, $\cos\theta$ is read as the radius of the $S^3$ wrapped by the D7-brane.

We apply an electric field in the $x^1$ direction. The $x^1$-component of the vector field is $A_1(t, z) = -Et + a_1(z)$ with an appropriate choice of the gauge. The action can be written as

$$S_{\mathrm{D7}} = -\mathcal{N}\int \mathrm{d}^4x\mathrm{d}z\cos^3\theta g_{xx}\sqrt{|g_{tt}|g_{xx}g_{zz} - (g_{zz}\dot{A}_1^2 - |g_{tt}|{A'_1}^2)}, \tag{3.37}$$

where $\mathcal{N} = \frac{\tau_7}{g_s}\mathrm{Vol}(S^3)$. The volume of the unit 3-sphere $\mathrm{Vol}(S^3)$ is given by $2\pi^2$. The equation of motion gives the constant of motion $J$ for $A_1$:

$$J = \frac{\mathcal{N}a_1'(z)|g_{tt}|g_{xx}\cos^3\theta}{\sqrt{|g_{tt}|g_{xx}g_{zz} - (g_{zz}E^2 - |g_{tt}|a_1'(z)^2)}}. \tag{3.38}$$

We find from (3.38) that

$$a_1'(z) = \frac{J}{\mathcal{N}}\sqrt{\frac{g_{zz}}{|g_{tt}|}}\sqrt{\frac{h(z)}{k(z)}}, \tag{3.39}$$

where $h$ and $k$ are defined by

$$h(z) \equiv |g_{tt}|g_{xx} - E^2, \tag{3.40a}$$

$$k(z) \equiv |g_{tt}|g_{xx}^3\cos^6\theta - g_{xx}J^2/\mathcal{N}^2. \tag{3.40b}$$

In the vicinity of $z = 0$, these functions are positive. On the other hand, the functions can be negative near the horizon for arbitrary $E$ and $J$. From the reality condition for $a_1$, there must be a turning point, say $z = z_*$, which satisfies

$$h(z_*) = k(z_*) = 0. \tag{3.41}$$

By definition, the position of $z_*$ is written as

$$\frac{z_*}{z_h} = \sqrt{\sqrt{1 + \frac{E^2}{\pi^4T^4}} - \frac{E}{\pi^2T^2}}. \tag{3.42}$$

$z_*$ can be also understood as a horizon of an analog black hole for the perturbation of the field on the D7-brane. We call $z = z_*$ as *effective horizon* in this thesis.

Note that $z_* = z_h$ when $E = 0$, and the effective horizon is equivalent to the black hole horizon at thermal equilibrium. However, they differ from each other when $\vec{J} \cdot \vec{E} \neq 0$.

The value of $J$ can be written in terms of $z_*$ from (3.41).

$$\begin{aligned} J =& \mathcal{N} \, |g_{tt}|^{1/2} g_{xx} \cos^3\theta \Big|_{z=z_*} \\ =& \mathcal{N} \pi T \sqrt[4]{1 + \left(\frac{E}{\pi^2 T^2}\right)^2} \cos^3\theta(z_*) E. \end{aligned} \tag{3.43}$$

This gives the expectation value of the current density in the $x^1$ direction. Then, the DC conductivity $\sigma_{\rm DC} \equiv J/E$ is written by

$$\sigma_{\rm DC} = \mathcal{N} \pi T \sqrt[4]{1 + \left(\frac{E}{\pi^2 T^2}\right)^2} \cos^3\theta(z_*), \tag{3.44}$$

which shows a nonlinear conductivity [11]. The field $\theta(z)$ is related to the mass of the charged particles. To obtain the conductivity for a specific mass, we have to solve $\theta(z)$ so that the mass of the charge carriers fixed at a designed value.

We derive the equation of motion for the scalar field $\theta(z)$. Let us consider a Legendre transform of DBI action called Routhian:

$$\begin{aligned} \tilde{S} \equiv& S_{\rm D7} - \int {\rm d}z F_{z1} \frac{\delta S_{\rm D7}}{\delta F_{z1}} \\ =& -\mathcal{N} \int {\rm d}^4x {\rm d}z \sqrt{\frac{g_{zz}}{|g_{tt}| g_{xx}}} \sqrt{(|g_{tt}| g_{xx} - E^2)(|g_{tt}| g_{xx}^3 \cos^6\theta(z) - g_{xx} J^2/\mathcal{N}^2)}. \end{aligned} \tag{3.45}$$

We obtain the equation of motion from Eq. (3.45) as:

$$\frac{\partial}{\partial z}\left(\theta'(z) \sqrt{\frac{h(z)k(z)}{|g_{tt}| g_{xx} g_z}}\right) - 3 \sin\theta \cos^5\theta \sqrt{|g_{tt}| g_{xx}^5 g_z \frac{h(z)}{k(z)}} = 0, \tag{3.46}$$

where $h(z)$ and $k(z)$ are defined by (3.40). The boundary condition for the scaler field at $z = z_*$ is given by taking the limit $z \to z_*$ of Eq. (3.46). The condition is written as

$$\theta'(z_*) = \frac{b - \sqrt{b^2 + c^2}}{z_* c}, \tag{3.47}$$

where

$$b \equiv 3 z_*^8 + 2 z_*^4 z_h^4 + 3 z_h^8, \quad c \equiv 3(z_*^4 - z_h^4)(z_*^4 + z_h^4) \tan\theta(z_*).$$

For $E = 0$, (3.47) simply gives $\theta'(z_* = z_h) = 0$. (3.47) means that $\theta'(z_*)$ is given in terms of $\theta(z_*)$, hence we obtain a unique solution once we determine the value of $\theta(z_*)$.

$\theta(z)$ in the vicinity of $z = 0$ is given by

$$\theta(z) = m_q z + \left( \frac{\langle \bar{\psi}\psi \rangle}{2\mathcal{N}} + \frac{m_q^3}{6} \right) z^3 + \cdots , \tag{3.48}$$

where $m_q$ is the mass of the charge carrier[4] and $\langle \bar{\psi}\psi \rangle$ is the chiral condensate. Therefore $m_q$ is determined if we assign the value of $\theta(z_*)$. We keep $m_q$ fixed at a designed value by choosing the value of $\theta(z_*)$ appropriately at each given value of $E$.

In the discussion above, we considered the configuration and the boundary condition for the D7-brane that goes into the (effective) horizon. Such a configuration is called as "black hole embedding" illustrated as iii) of Fig. 3.1. On the other hand, we can also consider the case of the D7-brane that does not touch the (effective) horizon. This configuration is called as "Minkowski embedding" illustrated as i) of Fig. 3.1. In this configuration, the radius of the $S^3$ part of the D7-brane vanishes at $0 \leq z < z_h$ and the D7-brane does not touch the horizon. In this configuration, $J$ is zero even in the presence of the electric field and the system is in equilibrium. For the embedding function $\theta$, the boundary condition for the Minkowski embedding is given by

$$\theta(z_0) = \frac{\pi}{2}, \quad \theta'(z_0) = \infty, \tag{3.49}$$

for arbitrary $z_0$ in $0 < z_0 < z_*$. We impose the second condition to avoid the conical singularity on the D7-brane's worldvolume.

### 3.3.1 Scaling symmetry

The D3-D7 model has a scalling symmetry. Let us consider the following transformations of the 4-dimensional Minkowski coordinates:

$$x^\mu \to a x^\mu, \tag{3.50}$$

where $a$ is a scaling constant. The metric (3.1) is unchanged under this transformation if we apply a transformation $w \to a^{-1} w$, simultaneously. For finite temperatures, the metric (3.33) is unchanged under this transformation with $z \to az$ and $z_h \to a z_h$. The quantities in the field theory also have similar scaling symmetry in this model. A quantity $Q$ which is transformed as $Q \to a^{-n} Q$ under (3.50) has the conformal dimension of $n$. For example, we find

$$m_q \to a^{-1} m_q, \quad \langle \bar{\psi}\psi \rangle \to a^{-3} \langle \bar{\psi}\psi \rangle , \quad F_{\mu\nu} \to a^{-2} F_{\mu\nu} \quad \langle J^\mu \rangle \to a^{-3} \langle J^\mu \rangle . \tag{3.51}$$

Then, we can always set one of these quantities to 1 by using the symmetry.

[4] The mass corresponds to the band gap in the condensed matter physics.

### 3.3.2 Negative differential conductivity

Let us analyze the $J$-$E$ characteristic. For this purpose, we compute the embedding function $\theta(z)$ from (3.46). In general, (3.46) can only be solved numerically because the equation is a nonlinear ODE. In the numerical computation, we must introduce a small cutoff at the regular singular points, $z = 0$ and $z_*$, to avoid numerical instabilities. We set the cutoff as $\varepsilon_{\rm IR} = \varepsilon_{\rm UV} = 0.00001 \times z_*$ for each configuration, where $\varepsilon_{\rm IR}$ and $\varepsilon_{\rm UV}$ are the cutoff at $z = z_*$ and that at $z = 0$, respectively. The integral region becomes $z = \varepsilon_{\rm UV}$ to $z = z_* - \varepsilon_{\rm IR}$. For simplicity, we set $\mathcal{N} = 1$.

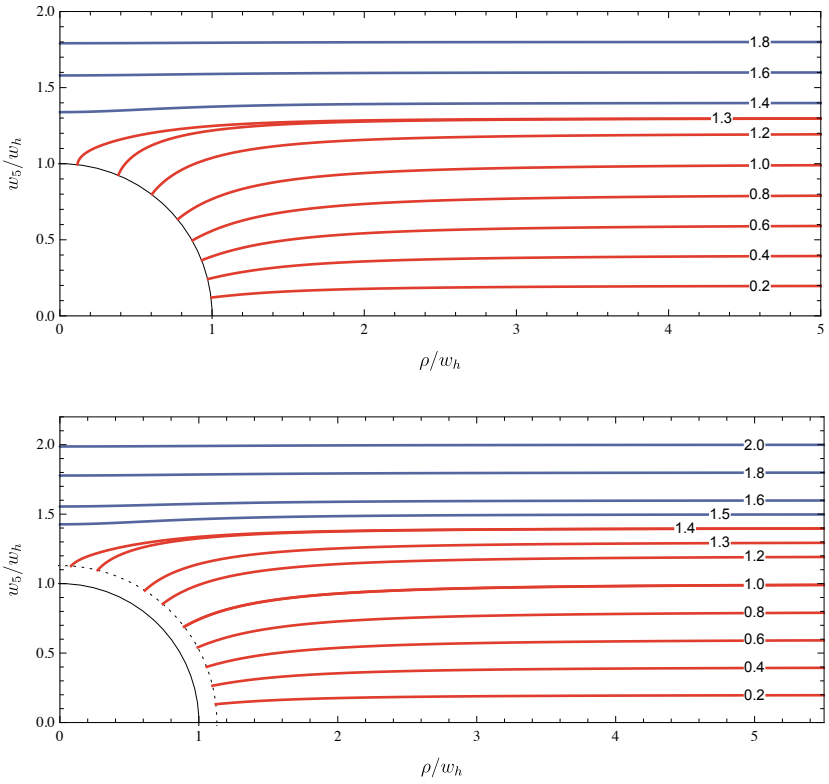


Figure 3.2: The embedding functions for various $m_q$ when $E = 0$ (top) and $E = 2.4339T^2$ (bottom). The labels overlaid on each line denote $\tilde{l}_q = w_5(\rho = \infty)/w_h$ corresponding to $m_q$. The red lines and the blue lines corresponds to the black hole embeddings and the Minkowski embeddings, respectively. The circle centered at the origin with radius 1 represents the black hole horizon. In the bottom panel, the dotted circle is the location of the effective horizon on the D7-brane's worldvolume.

Figure 3.2 shows numerical solutions of the brane embeddings obtained by solving (3.46). When $E = 0$, the solutions of the embedding functions are shown

in the top of Fig. 3.2. In this figures $\rho, w_5$ and $w_6$ are defined by

$$\rho = w\cos\theta, \quad w_5 = w\sin\theta\cos\psi, \quad w_6 = w\sin\theta\sin\psi \tag{3.52}$$

with $w = 1/z$. $w_h$ is given by $1/z_h$. In this coordinate, the background metric is written by

$$\mathrm{d}s_{10}^2 = w^2\left[-\frac{f(w)^2}{\tilde{f}(w)}\mathrm{d}t^2 + \tilde{f}(w)\mathrm{d}\vec{x}^2\right] + \frac{1}{w^2}\left[\mathrm{d}\rho^2 + \rho^2\mathrm{d}\Omega_3^2 + \mathrm{d}w_5^2 + \mathrm{d}w_6^2\right], \tag{3.53}$$

where $f(w) = 1 - w_h^4/w^4$ and $\tilde{f}(w) = 1 + w_h^4/w^4$. This expression of the metric is a finite temperature version of (3.1). In analogy with the zero temperature case, we read the quark mass by (3.4). Setting $(2\pi\alpha') = 1$, we obtain

$$m_q = w_5(\rho = +\infty). \tag{3.54}$$

In this figure, the embeddings are labeled by the value of $w_5/w_h$ at the boundary. For convenience, we write this dimensionless parameter as $\tilde{l}_q = w_5/w_h(\rho = \infty)$. This is related to the quark mass by $\tilde{l}_q = \sqrt{2}m_q/\pi T$. For $\tilde{l}_q \lesssim 1.2$, the solution is uniquely determined. Remarkably, there are two solutions for $\tilde{l}_q = 1.3$. These two solutions can be distinguished by $\theta(z_*)$ or other quantities like $\langle\bar{\psi}\psi\rangle$. Such a multi-valuedness against $m_q$ is observed in a very narrow range of $1.2966 < \tilde{l}_q < 1.3092$. $\tilde{l}_q = 1.3092$ is the upper bound for the black hole embeddings. When we consider larger mass than the upper bound, the solution is given by Minkowski embedding which does not touch the black hole.

For $E = 2.4339T^2$, the embeddings are shown in the bottom of Fig. 3.2. When $E > 0$, there is an effective horizon located outside the black hole horizon. The location of the effective horizon is shown as the dotted circle in the bottom of Fig. 3.2. We showed only the part of the embedding function outside the effective horizon, because the part of the embedding function inside the effective horizon does not affect to the boundary theory. For $\tilde{l}_q = 1.4$, there are two solutions existing, as we have for the case of $E = 0$. The multi-valuedness is observed in a rage of $1.3985 < \tilde{l}_q < 1.4025$ and $\tilde{l}_q = 1.4025$ is the upper bound in this case. The electric field applied to the system increases the upper bound of $\tilde{l}_q$ for the black hole embeddings.

Figure 3.3 shows the DC conductivity $\sigma_{\mathrm{DC}}/T$ given by (3.44) as a function of $m_q/T$ for various $E/T^2$. $\sigma_{\mathrm{DC}}$ is non-zero only in the black hole embeddings. The branch with $\sigma_{\mathrm{DC}}$ overlaying on the $x$-axis is the Minkowski embedding when $E = 0$. As shown in Fig. 3.2, the Minkowski embedding still exists even when we apply a finite electric field. The Minkowski embedding is considered as an insulator phase. In contrast, the black hole embedding is considered as the phase where the insulation is broken. We sometimes call it as "metallic" phase conventionally.

The $J$-$E$ characteristics in our system at various temperatures are given in Fig. 3.4. This results can be obtained by collecting the data at some fixed $m_q/T$ in Fig. 3.3. Notice that only scale-invariant quantities, such as $m_q/T$, are meaningful because of the scale symmetry. In other words, we can fix one of

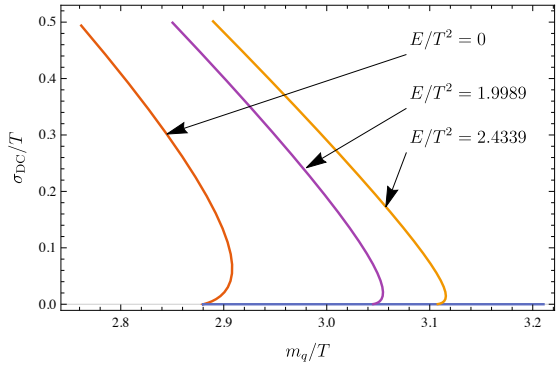


Figure 3.3: DC conductivity $\sigma_{\rm DC}/T$ as a function of $m_q/T$ for various $E/T^2$. The line with $\sigma_{\rm DC}/T = 0$ is the solutions in Minkowski embedding when $E = 0$.

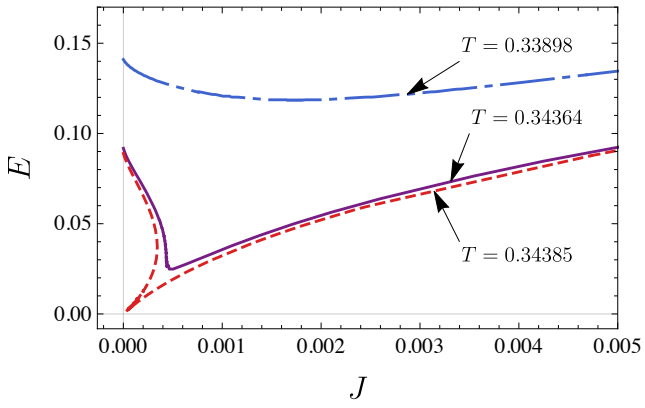


Figure 3.4: $J$-$E$ characteristics at various temperatures: from top to bottom $T = 0.33898, 0.34364, 0.34385$, respectively.[13] We have set $m_q = 1$ for simplicity.

the dimensionful quantities to 1 in this model. So we have fixed $m_q$ to 1. On $E$-axis with $J = 0$, there are solutions of the insulator phase at each temperature although we do not plot in the figure. The system is an insulator at vanishing charge density, but the insulation is broken by applying a strong electric field. In the phase where the insulation is broken, the charge carrier is provided by the pair-creation of the positively charged particle and negatively charged particle. In analogy with the electron-hole system, these particles correspond to the electron and the hole. In the small $J$ region, we can see a negative differential conductivity (NDC): $\partial J/\partial E < 0$ [5, 6].[5] For $T > 0.34385$, the $E$-$J$ characteristics reach the point $E = 0$ and $J = 0$ even in vanishing density. This is understood as a finite temperature effect. On the other hand, we can see a positive differential conductivity (PDC) for large $J$. For large $E$ or large $J$, the $J$-$E$ characteristics asymptotes to the behavior of $J \propto \mathcal{N} E^{3/2}$.

[5] It is known that a system which has such a NDC often shows instability called as filamentary instability [28]. There is a possibility that our system also shows the instability. It is interesting to investigate the instability however we don't consider the instability since we focus the homogeneous system in this thesis.

# Chapter 4

# Bound states in the holographic conductor

We analyze the behavior of the bound states in the holographic conductor.[13][1] The relationship between lifetime of the bound state and the applied electric field gives us a hint of the mechanism of the NDC. We find that when the system shows negative differential conductivity, the lifetime of the bound states grows as the electric field increases. The result suggests that the NDC in this system is realized by the suppression of the ionization of the bound states that supplies the free carriers.

## 4.1 Setup

The bound state in the boundary theory is realized as the normalizable mode of the perturbation field on a background configuration in the gravity theory. In this study, we consider a perturbation of the normalizable mode of the transverse vector field for simplicity, since it is decoupled from all other perturbation fields at the linear order of the equation of motion. Hereafter, we write the transverse direction as $x^\perp = x^{2,3}$. Behavior of the spectral function of $A_\perp$ has been studied in [29]. We analyze the behavior of the QNM of the perturbation field of $A_\perp$ in detail and clarify its dependence on $E$ in the NDC region.

The ansatz for the gauge fields is

$$A_a \mathrm{d}\xi^a \equiv (-Et + a_1(z))\mathrm{d}x^1 + \mathcal{A}(z,t)\mathrm{d}x^\perp, \tag{4.1}$$

where $\mathcal{A}(z,t)$ is the perturbation field of the transverse vector mode. We have set the transverse direction to $x^\perp$ direction without loss of generality. We assume the perturbation field is independent of the spatial coordinates $\vec{x}$.

The equations of motion for the gauge field are written as

$$\partial_b[\sqrt{-\det(g_{ab}+F_{ab})}g^{ac}F_{cd}\gamma^{db}] = 0, \tag{4.2}$$

[1] This work is based on a collaboration with S. Nakamura.

where $\gamma_{ab}$ is the *open string metric*: $\gamma_{ab} \equiv g_{ab} - F_{ac}g^{cd}F_{db}$. $\gamma^{ab}$ is defined by $\gamma^{ac}\gamma_{cb} = \delta^a{}_b$. For $A_\perp$, the linearized equation of motion becomes

$$\partial_b[\sqrt{-\det(g_{ab}+F_{ab})}g^{\perp\perp}\partial_d\mathcal{A}(z,t)\gamma^{db}] = 0. \tag{4.3}$$

We condider the Fourier transform of the gauge field, $\tilde{\mathcal{A}}(z,\omega) = \int_{-\infty}^{\infty} \mathrm{d}t \exp(i\omega t)\mathcal{A}(z,t)$. Then the equation of motion is written as

$$\begin{aligned}&\partial_z[\sqrt{-\det G_{ab}}g^{\perp\perp}(\gamma^{zz}\mathcal{A}'(z) - i\omega\gamma^{tz}\mathcal{A}(z))] \\ &\quad - i\omega\sqrt{-\det G_{ab}}g^{\perp\perp}\gamma^{tz}\mathcal{A}'(z) - \omega^2\sqrt{-\det G_{ab}}g^{\perp\perp}\gamma^{tt}\mathcal{A}(z) = 0,\end{aligned} \tag{4.4}$$

where $G_{ab} = g_{ab} + F_{ab}$. We simply wrote $\tilde{\mathcal{A}}(z,\omega)$ as $\mathcal{A}(z)$.

For the Mikowski ebeddings, we should impose the boundary condition for the perturbation field at $z = z_0$ as

$$\frac{\mathcal{A}'(z_0)}{\mathcal{A}(z_0)} = 0. \tag{4.5}$$

For the black hole embeddings, we must impose the ingoing-wave boundary condition at $z = z_*$ to obtain the proper solution. This is because the position of $z = z_*$ on the worldvolume of the D7-brane plays a role of the horizon for the perturbation field.

### 4.1.1 Ingoing-wave boundary condition with $J = 0$

Before we study the ingoing-wave condition in NESS with finite $J$, we consider the perturbation field in the background of $E = J = 0$. When we set $E = 0$, the location of the effective horizon $z = z_*$ and the open string metric $\gamma_{ab}$ reduce to the location of the black hole horizon $z = z_h$ and the induced metric $g_{ab}$, respectively. In such a background configuration, the perturbation field which we consider now has been studied in [26]. By using the expression for the induced metric (3.36), we write the linearized equation of motion as

$$\partial_z\left[\frac{f(z)}{z^2}\frac{\cos^3\theta(z)}{\sqrt{1/z^2+\theta'(z)^2}}\mathcal{A}'(z)\right] + \omega^2\frac{\tilde{f}(z)}{f(z)}\sqrt{\frac{1}{z^2}+\theta'(z)^2}\cos^3\theta(z)\mathcal{A}(z) = 0. \tag{4.6}$$

Let us perform the Frobenius expansion in the vicinity of $z = z_h$:

$$\mathcal{A}(z,\omega) = f(z)^\lambda(\hat{\mathcal{A}}_{(0)} + \mathcal{O}(1-z/z_h)). \tag{4.7}$$

Note that $f(z)$ is order of $\mathcal{O}(1-z/z_h)$. In the vicinity of $z = z_h$, the leading contribution of (4.6) is given by

$$\lambda^2\frac{f'(z_h)}{z_h^2} + \omega^2\frac{\tilde{f}(z_h)}{f'(z_h)}\left(\frac{1}{z_h^2}+\theta'(z_h)^2\right) = 0. \tag{4.8}$$

Recall that $\theta'(z_h) = 0$ when $E = 0$, then we find

$$\lambda = \pm i\frac{\omega}{2\pi T}. \tag{4.9}$$

Let us analyze these two solutions in the tortoise coordinates. In the vicinity of $z = z_h$, the tortoise coordinates is given by

$$\tilde{t} = t, \quad \bar{z} = \int_0^z \frac{\tilde{f}(z')^{1/2}}{f(z')} \mathrm{d}z' \simeq -\frac{1}{2\pi T} \log(1 - z/z_h). \tag{4.10}$$

Note that the horizon is located at $\tilde{z} = +\infty$ in the tortoise coordinate. The plane-wave ansatz is written as

$$\mathcal{A}(z) e^{-i\omega t} \simeq \hat{\mathcal{A}}_{(0)} (1 - z/z_h)^{\lambda} e^{-i\omega t} \simeq \hat{\mathcal{A}}_{(0)} \exp\left[-i(\omega \tilde{t} + 2\pi T \lambda \tilde{z})\right]. \tag{4.11}$$

For $\lambda = -i\omega/2\pi T$, the perturbation field propagates towards $\tilde{z} = +\infty$. Therefore, $\lambda = -i\omega/2\pi T$ and $+i\omega/2\pi T$ correspond to the ingoing-wave and outgoing-wave solutions, respectively.

By considering $\mathcal{A}(z) = f(z)^{\lambda} \hat{\mathcal{A}}(z)$ with $\lambda = -i\omega/2\pi T$, we write (4.6) as

$$\begin{aligned} &\partial_z \left[ \frac{f(z)}{z^2} \frac{\cos^3\theta(z)}{\sqrt{1/z^2 + \theta'(z)^2}} \left( \hat{\mathcal{A}}'(z) - i \frac{\omega}{2\pi T} \frac{f'(z)}{f(z)} \hat{\mathcal{A}}(z) \right) \right] \\ &- i \frac{\omega}{2\pi T} \frac{f'(z)}{z^2} \frac{\cos^3\theta(z)}{\sqrt{1/z^2 + \theta'(z)^2}} \left( \hat{\mathcal{A}}'(z) - i \frac{\omega}{2\pi T} \frac{f'(z)}{f(z)} \hat{\mathcal{A}}(z) \right) \\ &+ \omega^2 \frac{\tilde{f}(z)}{f(z)} \sqrt{\frac{1}{z^2} + \theta'(z)^2} \cos^3\theta(z) \hat{\mathcal{A}}(z) = 0. \end{aligned} \tag{4.12}$$

Now, the ingoing-wave boundary condition is replaced with the regularity condition at $z = z_h$. By solving (4.12) in the vicinity of $z = z_h$ with the regularity condition, we find

$$\frac{\hat{\mathcal{A}}'(z_h)}{\hat{\mathcal{A}}(z_h)} = \frac{i\omega}{\sqrt{2}}. \tag{4.13}$$

Since we are working on the linearized equation, $\hat{\mathcal{A}}(z_h)$ is just a normalization constant of $\hat{\mathcal{A}}(z)$.

### 4.1.2 Ingoing-wave boundary condition in NESS

Let us consider the ingoing-wave condition for the perturbation field in the NESS background. In the presence of $\vec{J} \cdot \vec{E}$, we need to impose the ingoing-wave boundary condition not at the location of the black hole horizon but at the effective horizon. By performing the Frobenius expansion in the vicinity of $z = z_*$, we write

$$\mathcal{A}(z, \omega) = (1 - z/z_*)^{\lambda} (\mathcal{A}_{(0)} + \mathcal{O}(1 - z/z_*)). \tag{4.14}$$

$\lambda$ is determined by (4.4). Note that $\gamma^{zz}$ goes to zero whereas $\gamma^{tz}$ and $\gamma^{tt}$ do not vanish at $z = z_*$. Then we find that $\lambda$ must satisfy

$$\lambda \left( \lambda - 2i\omega \left. \frac{\gamma^{tz}}{(\gamma^{zz})'} \right|_{z_*} \right) = 0. \tag{4.15}$$

We obtain two distinct solutions:

$$\lambda_- = 0, \quad \lambda_+ = 2i\omega\, \gamma^{tz}/(\gamma^{zz})'\big|_{z_*} = -2i\omega \frac{a_1'}{(|g_{tt}|g_{xx})'}(z_*). \tag{4.16}$$

$\lambda_-$ corresponds to the ingoing-wave boundary condition because of the following reasons. The equation of motion of the perturbation field is described by using the open string metric $\gamma_{ab}$, which has off-diagonal components $\gamma_{tz} = \gamma_{zt}$ in our setup. The open string metric can be diagonalized as

$$\gamma_{ab}\mathrm{d}\xi^a\mathrm{d}\xi^b = |\gamma_{tt}| \left[ -\left( \mathrm{d}t - \frac{\gamma_{tz}}{|\gamma_{tt}|}\mathrm{d}z \right)^2 + \frac{1}{|\gamma_{tt}|}\left( \gamma_{zz} + \frac{\gamma_{tz}^2}{|\gamma_{tt}|} \right) \mathrm{d}z^2 \right] + \cdots . \tag{4.17}$$

We consider a conformally flat coordinates

$$\tilde{t} = t - \int_0^z \frac{\gamma_{tz}}{|\gamma_{tt}|}\mathrm{d}z', \quad \tilde{z} = -\int_0^z \sqrt{\frac{1}{|\gamma_{tt}|}\left( \gamma_{zz} + \frac{\gamma_{tz}^2}{|\gamma_{tt}|} \right)}\mathrm{d}z', \tag{4.18}$$

so that we have

$$\gamma_{ab}\mathrm{d}\xi^a\mathrm{d}\xi^b = |\gamma_{tt}| \left( -\mathrm{d}\tilde{t}^2 + \mathrm{d}\tilde{z}^2 \right) + \cdots . \tag{4.19}$$

In the vicinity of $z = z_*$, we have

$$\tilde{t} = t - \left. \frac{\gamma_{tz}}{|\gamma_{tt}|'} \right|_{z_*} \log|1 - z/z_*|, \quad \tilde{z} = -\left. \frac{\gamma_{tz}}{|\gamma_{tt}|'} \right|_{z_*} \log|1 - z/z_*|. \tag{4.20}$$

The perturbation field in the vicinity of $z = z_*$ is now given by

$$\begin{aligned} \mathcal{A}(z,\omega)e^{-i\omega t} \simeq & \mathcal{A}_{(0)} \exp\left[ -i\omega t + \lambda_\pm \log(1 - z/z_*) \right] \\ = & \mathcal{A}_{(0)} \exp\left[ -i\omega(\tilde{t} \pm \tilde{z}) \right], \end{aligned} \tag{4.21}$$

where the double sign corresponds to that of $\lambda_\pm$ respectively. Since the effective horizon is at $\tilde{z} = +\infty$, the ingoing wave solution is $\mathcal{A}_{(0)} \exp\left[ -i\omega(\tilde{t} - \tilde{z}) \right] = \mathcal{A}_{(0)} \exp\left[ -i\omega t \right]$.

In [29], it is also argued that $\lambda_-$ corresponds to the ingoing wave boundary condition in view of the consistency in the limit of $E \to 0$. Let us perform the Frobenius expansion in the vicinity of the black hole horizon $z = z_h$:

$$\mathcal{A}(z,\omega) = (1 - z/z_h)^{\tilde{\lambda}} \left( \tilde{\mathcal{A}}_{(0)} + \mathcal{O}(1 - z/z_h) \right). \tag{4.22}$$

Then, the equation of motion gives the two distinct solutions for $\tilde{\lambda}$:

$$\tilde{\lambda}_\pm = \frac{1 \pm 1}{2} + i\omega \frac{f(z)}{f'(z)} \left. \frac{a_1'(z)}{E} \right|_{z=z_h}. \tag{4.23}$$

Since $a_1'(z)$ is proportional to $1/f(z)$, the second term converges to a finite value. One find that the value of the Frobenius exponent at $z = z_h$ is different from (4.9) for $E = 0$. Unlike the case of $E = 0$, the black hole horizon is hidden by

the effective horizon from the point of view of the observers outside the effective horizon on the worldvolume. In the vicinity of the $z = z_*$, we have also two choices of the Frobenius exponent $\lambda$.

Let us see the behavior of the perturbation fields in a limit of $E \to 0$ for each choice of the Frobenius exponents. For finite $E$, we write

$$\mathcal{A}(z,\omega) = (1 - z/z_h)^{\tilde{\lambda}}(1 - z/z_*)^{\lambda}\mathcal{A}_{\rm reg}(z,\omega), \tag{4.24}$$

where $\mathcal{A}_{\rm reg}(z,\omega)$ is a regular function at $z = z_h$ and $z = z_*$. Since $z_*$ reduces to $z_h$ in the limit of $E = 0$, we expect there is $\lambda_{\rm tot}$ which is defined by

$$(1 - z/z_h)^{\lambda_{\rm tot}}\mathcal{A}_{\rm reg}(z,\omega) \equiv \lim_{E\to 0}(1 - z/z_h)^{(\tilde{\lambda}+\lambda)}\mathcal{A}_{\rm reg}(z,\omega). \tag{4.25}$$

In the limit of $E = 0$, $\lambda_+$ must be

$$\lim_{E\to 0}\lambda_+ = i\frac{\omega}{2\pi T}. \tag{4.26}$$

(4.23) gives us

$$\lim_{E\to 0}\tilde{\lambda}_\pm = \frac{1 \pm 1}{2} - i\frac{\omega}{2\pi T}. \tag{4.27}$$

There are four possible combinations of each two values of the Frobenius exponents:

$$\lim_{E\to 0}\tilde{\lambda}_+ + \lambda_+ = 1 \tag{4.28a}$$

$$\lim_{E\to 0}\tilde{\lambda}_+ + \lambda_- = 1 - i\frac{\omega}{2\pi T}, \tag{4.28b}$$

$$\lim_{E\to 0}\tilde{\lambda}_- + \lambda_+ = 0, \tag{4.28c}$$

$$\lim_{E\to 0}\tilde{\lambda}_- + \lambda_- = -i\frac{\omega}{2\pi T}. \tag{4.28d}$$

In the case of $E = 0$, the exponent $-i\frac{\omega}{2\pi T}$ corresponds to the ingoing wave and $i\frac{\omega}{2\pi T}$ does outgoing wave. (4.28d) is exactly the exponent which realizes the ingoing-wave solution.[2] By the consistency, we regard the choice of $\lambda_-$ at $z = z_*$ corresponds to the ingoing-wave boundary condition. The result agrees with the previous discussion based on the open string metric.

Once the Frobenius exponent is determined, the ingoing-wave boundary condition can be replaced with the regularity condition at $z = z_*$. Since $\gamma^{zz}$ vanishes at $z = z_*$, we obtain

$$\frac{\mathcal{A}'(z_*)}{\mathcal{A}(z_*)} = \left.\frac{i\omega(\sqrt{-\det G_{ab}}g^{\perp\perp}\gamma^{tz})'/\sqrt{-\det G_{ab}}g^{\perp\perp} + \omega^2\gamma^{tt}}{(\gamma^{zz})' - 2i\omega\gamma^{tz}}\right|_{z=z_*}. \tag{4.29}$$

[2] We can not find the outgoing mode in (4.28). In [30], they found both of the ingoing- and outgoing- modes in the total Frobenius exponents in a limit of $E \to 0$. They used another coordinate system, and they obtained the exponents corresponding to the ingoing- and outgoing-wave as $\lambda = \pm i\omega/4\pi T$. The Frobenius exponents depend on the choice of the coordinates.

In order to study the corresponding bound state, we also need to impose the vanishing condition at the boundary: $\mathcal{A}(0) = 0$ at $z = 0$. This condition ensures that the solution is a resonance state without an external source, in other words a bound state. The equation of motion with the boundary conditions at two boundaries provides us an eigenvalue problem.

### 4.1.3 AC conductivity

We make a comment on the computation of the spectral function for the perturbation field discussed in Ref. [29]. Let us consider the on-shell action obtained from (3.35), whose relevant term is given by

$$S_{\rm D7}^{\text{on-shell}} \simeq -\frac{\mathcal{N}}{2}\int \mathrm{d}^4x\ \sqrt{-\det G_{ab}}g^{\perp\perp}\gamma^{zz}\mathcal{A}'(t,z)\mathcal{A}(t,z)\Big|_{z=0}. \tag{4.30}$$

We dropped the surface term at $z = z_h$ in accordance with the Minkowskian prescription of the AdS/CFT correspondence [31]. Following [31], the current-current two-point function is given by

$$G^{\rm R}_{\perp\perp}(\omega) = \mathcal{N}\sqrt{-\det G_{ab}}g^{\perp\perp}\gamma^{zz}\ \frac{\mathcal{A}'(z,\omega)\mathcal{A}(z,\omega)^*}{|\mathcal{A}(z,\omega)|}\Big|_{z=0}, \tag{4.31}$$

where $\mathcal{A}(z,\omega)$ is the Fourier transform of $\mathcal{A}(z,t)$. From this expression, we can see that the Dirichlet condition at $z = 0$, $\mathcal{A}(0) = 0$, makes $G^{\rm R}_{\perp\perp}(\omega)$ divergent. This implies QNMs correspond to the poles of the two-point function. By using the Kubo formula, we obtain the $x^\perp$-$x^\perp$ components of the AC conductivity tensor as

$$\sigma^{\perp\perp}(\omega) = -\frac{\mathrm{Im}G^{\rm R}_{\perp\perp}(\omega)}{\omega}. \tag{4.32}$$

We demonstrate (4.32) gives the expression of the DC conductivity given by (3.44) in the limit of $\omega \to 0$.[29] Let us expand the perturbation field with respect to $\omega$:

$$\mathcal{A}(z,\omega) = \mathcal{A}_{(0)}(z) + \omega\mathcal{A}_{(1)} + \mathcal{O}\big(\omega^2\big), \tag{4.33}$$

where $\mathcal{A}_{(k)}(z)$ is order of $\omega^k$. In the 0-th order of $\omega$, (4.4) gives

$$\partial_z\left[\sqrt{-\det G_{ab}}g^{\perp\perp}\gamma^{zz}\mathcal{A}'_{(0)}(z)\right] = 0. \tag{4.34}$$

The solution is written as

$$\mathcal{A}_{(0)}(z) = C_{(0)} + \tilde{C}_{(0)}\int_{z_*}^{z}\frac{\mathrm{d}z'}{\sqrt{-\det G_{ab}}g^{\perp\perp}\gamma^{zz}}. \tag{4.35}$$

$C_{(0)}$ and $\tilde{C}_{(0)}$ are integration constants. The second term is divergent at $z = z_*$ since $\gamma^{zz}$ goes to zero. From the regularity condition for $\mathcal{A}(z)$, we set $\tilde{C}_{(0)} = 0$. At the 1st order of $\omega$, the equation is given by

$$\partial_z\left[\sqrt{-\det G_{ab}}g^{\perp\perp}\left(\gamma^{zz}\mathcal{A}'_{(1)}(z) - i\omega\gamma^{tz}C_{(0)}\right)\right] = 0. \tag{4.36}$$

We obtain the solution

$$\mathcal{A}_{(1)}(z) = \int_{z_*}^{z} \frac{C_{(1)} + i\omega\sqrt{-\det G_{ab}}g^{\perp\perp}\gamma^{tz}C_{(0)}}{\sqrt{-\det G_{ab}}g^{\perp\perp}\gamma^{zz}}\mathrm{d}z' + \tilde{C}_{(1)}, \tag{4.37}$$

where $C_{(1)}$ and $\tilde{C}_{(1)}$ are integration constants which have order of $\omega$. We must make the solution regular. To do this, we set

$$C_{(1)} = i\omega\sqrt{-\det G_{ab}}g^{\perp\perp}\gamma^{tz}\Big|_{z=z_*} C_{(0)}. \tag{4.38}$$

Then, the first term in (4.37) is convergent at $z = z_*$. Setting $\mathcal{A}(z_*) = C_{(0)}$, we can fix $\tilde{C}_{(1)}$ to zero without loss of generality. By inserting these results to (4.32), we obtain

$$\begin{aligned}\sigma^{\perp\perp}(\omega = 0) =& -\mathcal{N}\lim_{\omega\to 0}\mathrm{Im}\left[\frac{C_{(1)} + i\omega\sqrt{-\det G_{ab}}g^{\perp\perp}\gamma^{tz}C_{(0)}}{\omega C_{(0)}}\right]_{z=0} \\ =& -\mathcal{N}\left[\sqrt{-\det G_{ab}}g^{\perp\perp}\gamma^{tz}\Big|_{z=z_*} + \sqrt{-\det G_{ab}}g^{\perp\perp}\gamma^{tz}\Big|_{z=0}\right].\end{aligned} \tag{4.39}$$

(4.39) is computed by using the following formula:

$$\begin{aligned}\mathcal{N}\sqrt{-\det G_{ab}}g^{\perp\perp}\gamma^{tz} =& \frac{-\mathcal{N}Ea_1'(z)\cos^3\theta}{\sqrt{|g_{tt}|g_{xx}g_{zz} - (g_{zz}E^2 - |g_{tt}|a_1'(z)^2)}} \\ =& -\frac{JE}{|g_{tt}|g_{xx}}.\end{aligned} \tag{4.40}$$

In the second line, we used (3.38). Evaluating this function at $z = 0$, one finds the second term in the parenthesis in (4.39) vanishes. From the first term, we find

$$\sigma^{\perp\perp}(\omega = 0) = \frac{J}{E} = \sigma_{\mathrm{DC}}. \tag{4.41}$$

We used the relationship (3.41) at $z = z_*$.

## 4.2 Numerical results

In this section we show the numerical results of the analysis of the QNMs. In Section 4.2.3, we show the relationship between the lifetime of the bound state and the electric field. We find the the mechanism of NDC is related to by the decay process of the bound states.

### 4.2.1 The behavior of the perturbation field in the holographic conductor

In this section, we explain the behavior of the solutions of (4.4) and the details of the numerical computation. We can not solve (4.4) analytically, because the

equation involves $\theta$ which can be obtained numerically. In order to stabilize the numerical computations, we introduce cutoff s at the regular-singular points $z = 0$ and $z = z_*$.

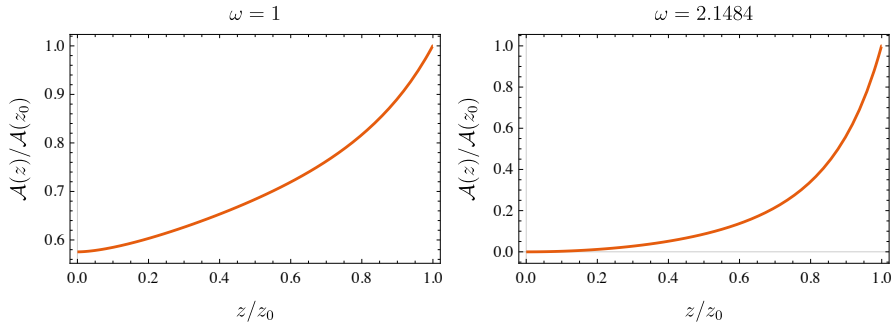


Figure 4.1: (Left) Solution of the perturbation field at $\omega = 1$. (Right) Solution of the perturbation field at $\omega = 2.1484$. This frequency corresponds to the lowest value of the normal frequencies indicated by cyan circle in Fig. 4.2. This solution gives the lowest normal mode. In both cases, the background configuration is classified as the Minkowski embedding which is parameterized by $E = 0.051567$ at $T = 0.34364$.

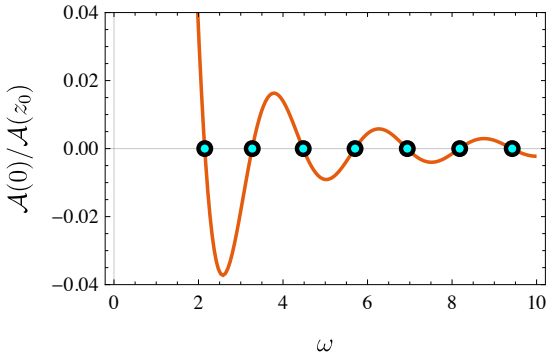


Figure 4.2: $\mathcal{A}(0)/\mathcal{A}(z_0)$ as a function of $\omega$ at $E = 0.051567$ and $T = 0.34364$. The cyan circles indicate the zero points of this function. They correspond to the normal modes.

Let us begin with the analysis for the insulator phase that is realized by the Minkowski embeddings. We solve the equation of motion (4.4) under the boundary condition (4.5). The obtained solutions are plotted in Fig. 4.1. In the Minkowski embeddings, the solution of the perturbation field has no imaginary part. The left panel of Fig. 4.1 shows an example of solution at $\omega = 1$. The solution does not satisfy the Dirichlet condition $\mathcal{A}(0) = 0$ but has finite value of $\mathcal{A}(0)/\mathcal{A}(z_0) \approx 0.59$ at $z = 0$. This means that $\omega = 1$ is not the eigenvalue. In the

right panel of Fig. 4.1, the solution satisfies the Dirichlet condition at $z = 0$ for $\omega = 2.1484$. We used `FindMinimum` built-in function in *Wolfram Mathematica 12* to find the $\omega$ that satisfies the condition above. This solution is the normal mode with the normal frequency of $\omega = 2.1484$. The normal mode is interpreted as the bound state and the normal frequency gives the mass of the bound state. The two-point boundary value problem has the family of solutions $\mathcal{A}(z)$ with eigenvalues of $\omega$. Fig. 4.2 shows $\mathcal{A}(0)/\mathcal{A}(z_0)$ as a function of $\omega$. The zero points of this function indicated by the cyan circles corresponds to the normal frequencies. There is an infinite tower of the normal modes similar to (3.17). All the normal frequencies are real in this case. The reality of the normal frequency implies that the bound states have infinite lifetime in this phase.

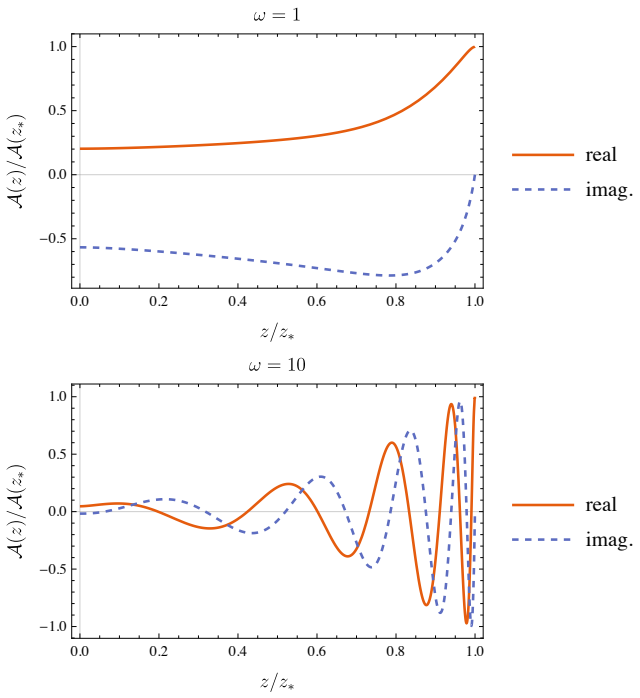


Figure 4.3: Solutions for (4.4) with $\omega = 1$ (top) and $\omega = 10$ (bottom). The red line and blue dotted line correspond to the real part and the imaginary part of the field, respectively. Here, $J = 0.0020000, E = 0.051567$ at $T = 0.34364$ corresponding to the purple line in Fig. 3.4.

Next, let us consider the perturbation field in the conductor phase. Imposing the regular boundary condition at $z = z_*$ given by (4.29), we solve the equation of motion (4.4). The solutions of the perturbation field in the black hole embedding are shown in Fig. 4.3. In contrast to the case of the insulator phase, the solutions of the perturbation field have finite imaginary part. Moreover, there is no regular solution satisfying the boundary condition at $z = 0$ for purely real-valued $\omega$. In

general, it is known that the eigenvalue of $\omega$ is complex for the a black hole embeddings. The corresponding mode is reffered *quasinormal mode* (QNM). We call the complex-valued eigenvalue of $\omega$ as *quasinormal frequency*. The imaginary part of the quasinormal frequency originates in the non-Hermitian aspect of the ingoing-wave boundary condition at the horizon.

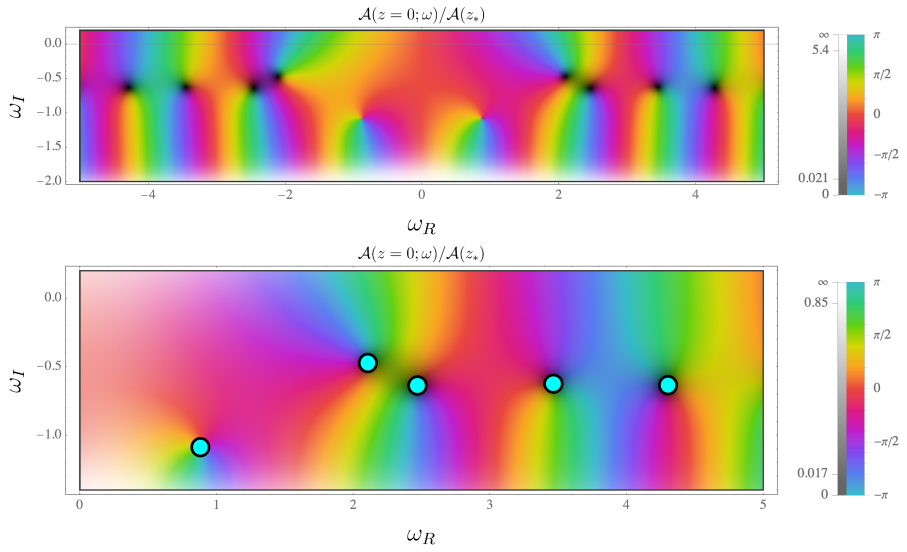


Figure 4.4: Plots of $\mathcal{A}(0;\omega)/\mathcal{A}(z_*)$ as a complex function of $\omega = \omega_R + i\omega_I$. The absolute value and the argument of the function are shown as a brightness and a hue at each point, respectively. The background configuration is the same as that of Fig. 4.3. The lower panel shows the right-half plane of the upper panel. In the lowe panel, the cyan circles indicate the locations of the QNMs where $\mathcal{A}(0)/\mathcal{A}(z_*)$ vanishes, namely the quasinormal frequencies.

Figure 4.4 shows the plots of $\mathcal{A}(0;\omega)/\mathcal{A}(z_*)$ on the complex $\omega$ plane, where $\omega = \omega_R + i\omega_I$. From the upper panel of Fig. 4.4, the function seems to be symmetric under the flip of the sign of $\omega_R$, thus we focus on the QNMs with $\omega_R > 0$. In the lower panel of Fig. 4.4, there are points indicated by cyan circles where $\mathcal{A}(0)/\mathcal{A}(z_*)$ vanishes. All these points lie in the region of $\omega_I < 0$. Therefore, the locations of the cyan circles correspond to the eigenvalues of the QNMs, namely quasinormal frequencies. In Fig. 4.4, we have shown only few modes for small $\omega_R$. It is seems that there is infinite tower of QNMs as is the case of (3.32). We compute the quasinormal frequency numerically by solving (4.4) with imposing the regularity condition at $z = z_*$ to $z = 0$ and finding $\omega$ that satisfies the boundary condition at $z = 0$.[3] This method is called *shooting*

[3]In the numerical computation, we regard that the Dirichlet condition is satisfied if

$$\left|\frac{\mathcal{A}(\varepsilon_{\rm UV})}{\mathcal{A}(z_* - \varepsilon_{\rm IR})}\right|(\omega) \lesssim 10^{-8}.$$

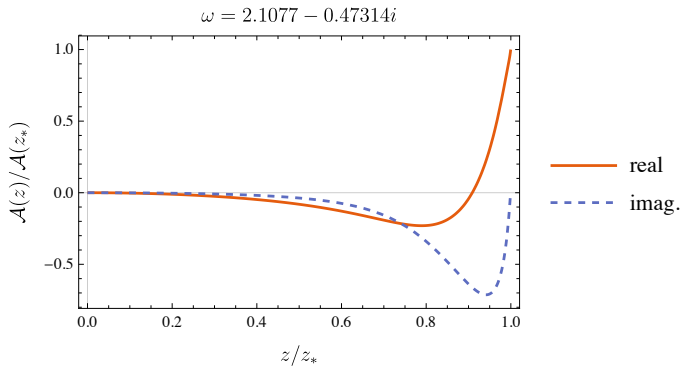


Figure 4.5: Solution corresponding to the lowest QNM with $\omega = 2.1077 - 0.47314i$, in Fig. 4.4. The solution satisfies both of the regular condition at $z = z_*$ and the vanishing Dirichlet condition at $z = 0$.

*method*.[4]

In Fig. 4.4, the quasinormal frequency at $\omega = 2.1077 - 0.47314i$ corresponds to the lowest QNM in this configuration.[5] Fig. 4.5 shows the corresponding eigen-solution for the lowest QNM. The solution satisfies both of the regularity condition at $z = z_*$ and the Dirichlet condition at $z = 0$. Here, the quasinormal frequency has the finite real part and the negative imaginary part. This means the mode shows damped odcillation. Such a behavior is called as *ringing down* in the context of the gravity physics and cosmology. The negative-imaginary part corresponds to the damping factor. In the viewpoint of the dual field theory, $-\omega_I$ is just proportional to the decay width of the corresponding bound state whose interpolating operator is $\bar{\psi}\gamma^{\perp}\psi$. In other words, it is known the quasinormal frequencies correspond to the poles of the retarded Green functions in the context of the AdS/CFT correspondence. Thus, we regard $-\omega_I$ as the decay width, namely the inverse of the lifetime of the bound state. In the next section, we show the behavior of the bound states by investigating the relationship between the lifetime and the applied electric field.

### 4.2.2 The behavior of the bound states for $E = 0$

When $E = 0$, the perturbation field can be either a normal mode or a QNM. Before presenting the result for $E > 0$, we check the consistency of our numerical calculation by comparing the analytic result in the cases of $E = 0$. In Fig. 4.6, we show the frequency of the lowest normal mode and the quasinormal mode as

We used `FindMinimum` built-in function in *Wolfram Mathematica 12* to find the $\omega$ that satisfies the condition above.

[4]It has been found that the numerical errors in the shooting method are large in the D3-D7 model when $|\omega_I|$ is greater than the order of the temperature [32]. However, we study only small region of $|\omega_I|$ in this thesis.

[5]More precisely, we can say this is the most stable QNM in this background configuration.

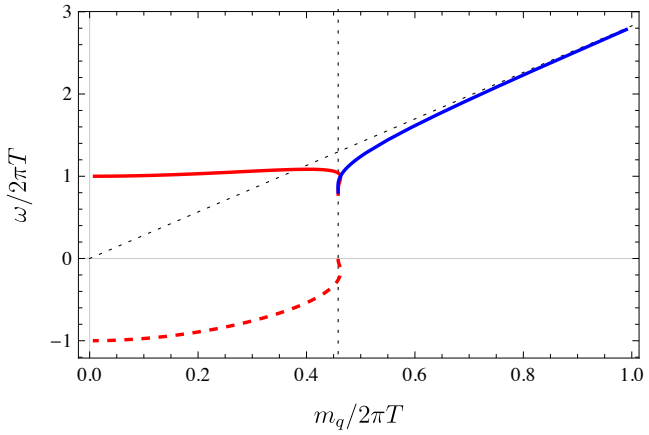


Figure 4.6: Frequency of the lowest (quasi-)normal mode as a function of $m_q/2\pi T$ when $E = 0$. The red line and red dashed line are corresponding to the real part and imaginary part of the quasinormal frequency in the black hole embedding. The blue line represents the normal frequency of the lowest normal mode in the Minkowski embedding. The vertical dotted line at $m_q/2\pi T = 0.45843$ indicates the point where the black hole embedding and the Minkowski embedding meet. Another dotted line shows the line of $\omega = 2\sqrt{2}m_q$.

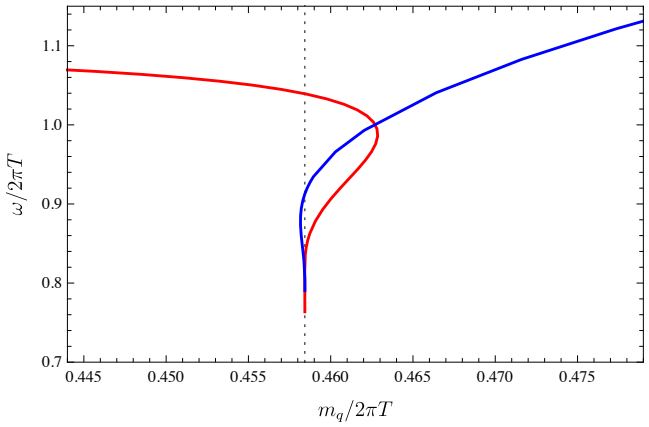


Figure 4.7: Detail of the solutions shown in Fig. 4.6 around $m_q/2\pi T = 0.45843$. The red line is the real part of the quasinormal frequency of the lowest QNM in the black hole embedding. The blue line is the normal frequency of the lowest mode in the Minkowski embedding. The vertical dotted line indicates the point where the two embeddings meet: $m_q/2\pi T = 0.45843$.

a function of $m_q/T$. In this subsection, we don't set $m_q = 1$ but keep it as a variable. For small $m_q/2\pi T$, the solution is given by the black hole embedding. The mode becomes the QNM. In the massless limit, the quasinormal frequency asymptotes to the analytic result (3.32): $\omega = 2\pi T(1-i)$. On the other hand, the solution is given by the Minkowski embedding for large $m_q/2\pi T$. In Fig. 4.6, we find the blue curve asymptotes to the line of $\omega = 2\sqrt{2}m_q$. This is consistent with the analytic result (3.18), $\omega = 2\sqrt{2}l_q/L^2$, with $l_q = m_q$ and $L = 1$.

Let us make a comment on the transition point between the black hole embedding and the Minkowski embedding. The transition point is located around $m_q/2\pi T = 0.45843$. Fig. 4.7 shows the behavior of the lowest (quasi-)normal mode versus $m_q/2\pi T$ near the transition point. In the vicinity of the transition point, however, the calculation is difficult owing to numerical errors. We can not see the convergence of the real part of the frequency of the lowest normal mode and QNM. It is interesting to understand the precise behavior of these solutions around the transition point.

### 4.2.3 The behavior of the bound states in the NDC region

In this subsection, we present how the lifetime of the bound state depend on the applied electric field $E$ when the system exhibit NDC. Since the lifetime is inversely proportional to $\omega_I = \mathrm{Im}\omega$ of the quasinormal frequency, we investigate $E$ dependence of $\omega_I$.[13]

We have computed $\omega_R$ and $\omega_I$ of the first excited mode of the transverse vector field as functions of $E$ and $J$ at various temperatures. In Fig. 4.8, Fig. 4.9 and Fig. 4.10, the dash-dot line, the solid line, and the broken line represent the data at $T = 0.33898, 0.34364$ and $0.34385$, respectively. The $J$-$E$ characteristics at the same temperatures are given in Fig. 3.4.

The location of the pole corresponding to the QNM is given in Fig. 4.8. The top and the bottom panel of the figure show the results in different ranges of $\omega = \omega_R + i\omega_I$. The pole moves along the curve at each temperature when we vary $E$ and $J$ along the corresponding $J$-$E$ curve in Fig. 3.4. The dotted line is a reference which indicates the location of the pole at $E = 0$ for various temperatures. The data used in the reference line is the same as the red line and red dotted line in Fig. 4.6. The reference line asymptotes to the analytical result (3.32) with $l = 0$ in the massless cases: $\omega/T = 2\pi(1-i)$, at the high temperature limit. Note that the broken line at $T = 0.33898$ touches the reference line of $E = 0$. This is because the $J$-$E$ characteristics at this temperature reaches $E = 0$ as shown in Fig. 3.4.

Let us see the details of the behavior of the lifetime of the bound states under the presence of $E$. The top panel of Fig. 4.9 shows the $J$-$E$ characteristics and the bottom panel shows the relationship between $-\omega_I$ and the electric field $E$. $-\omega_I$ is regarded as the decay width of the bound state. Note that $J$ and $-\omega_I$ are multi-valued functions of $E$. The branches of the smaller value of $-\omega_I$ correspond to the branches of smaller $J$. For the solid line and the dash-dot line, the smaller-$J$ branches always show NDC. We find that $\partial(-\omega_I)/\partial E < 0$ for these branches. *The fact that $\partial(-\omega_I)/\partial E$ turns into negative when the system*

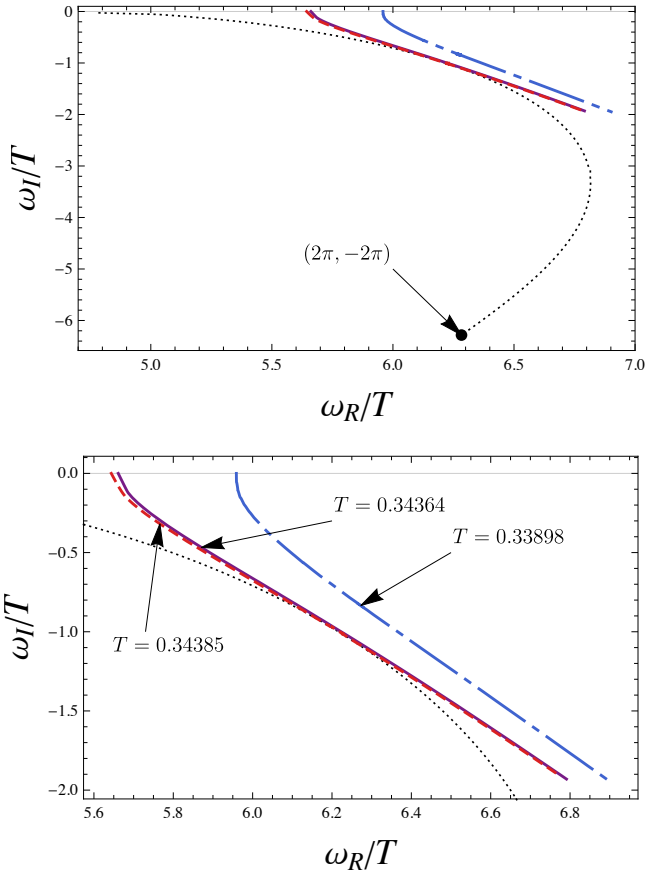


Figure 4.8: Trajectories of the poles at fixed temperatures when we vary $E$ and $J$ along the corresponding $J$-$E$ curve in Fig. 3.4.[13] The dotted line is a reference line at $E = 0$ for various temperatures. In the upper panel, we show whole range of the reference line at $E = 0$. The reference line asymptotes to the analytic result of $\omega = 2\pi T(1 - i)$ in the limit of high temperature. Same result for vanishing $E$ has been obtained in Ref. [32]. In the lower panel, we show the relevant region to the $E > 0$ cases. The upper endpoints with $\omega_I = 0$ are corresponding to the endpoints with $J = 0$ in Fig. 3.4.

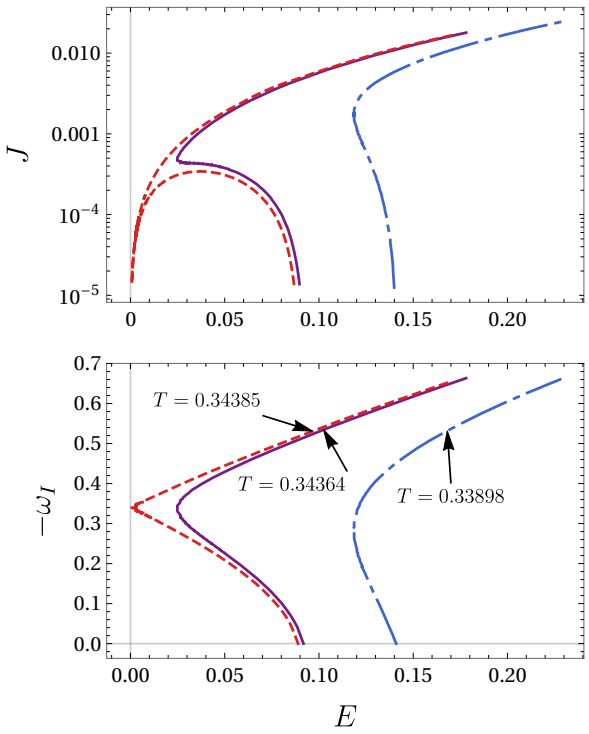


Figure 4.9: (top) $E$ dependence of $J$, (bottom) $-\omega_I$ as a function of $E$ at various temperatures.[13]

*shows NDC is the main result of our analysis.*

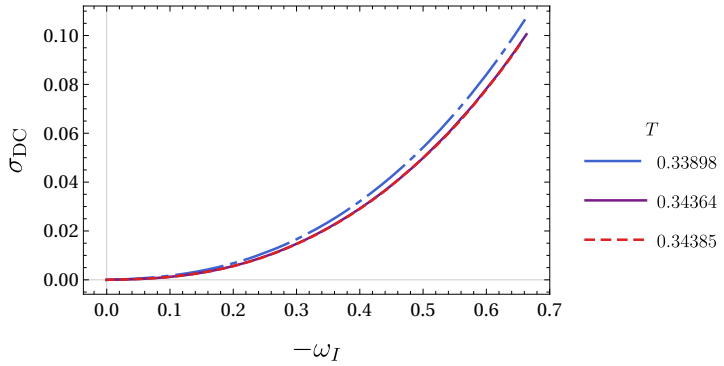


Figure 4.10: DC conductivity $\sigma_{\rm DC}$ vs. decay width $-\omega_I$ at various temperatures.[13] The lower two lines are almost overlapping.

Let us find the physical implication of this result. It is helpful to see Fig. 4.10 for this purpose. Fig. 4.10 shows the relationship between the decay width $-\omega_I$ and the DC conductivity $\sigma_{\rm DC}$ given in (3.44). $-\omega_I$ is a monotonically increasing function of $\sigma_{\rm DC}$ irrespective of the temperature. $\sigma_{\rm DC}$ seems to be proportional to the square power of $-\omega_I$: $\sigma_{\rm DC} \propto (-\omega_I)^2$. In particular, $\sigma_{\rm DC}$ reaches zero when $-\omega_I = 0$: we do not have electric conduction if the bound state is completely stable. This shows that the electric conduction in the vicinity of $\sigma_{\rm DC} = 0$ in the present system is owing to the charge carriers supplied by the ionization of the bound states. Now the physical implication of our result becomes clear. In the vicinity of $\sigma_{\rm DC} = 0$, the charge carriers are supplied by the ionization of the bound states. Let us focus on the $J$-$E$ characteristics *in the vicinity of* $\sigma DC = 0$ in Fig. 4.9. We should refer to the data where $E$ remains finite when $J$ approaches zero there. One finds that the data in the vicinity of $\sigma_{\rm DC} = 0$ show NDC, and $\partial(-\omega_I)/\partial E < 0$. These observations lead us to the conclusion that *the origin of the NDC in the present system is suppression of the ionization of the bound states which provides the charge carriers, by the increase of the electric field.*

Let us make a few comments. Our statement is that when we have NDC, $\partial(-\omega_I)/\partial E < 0$. However we do *not* claim that whenever $\partial(-\omega_I)/\partial E < 0$ is realized the system always shows NDC. For example, the lower branch of the broken line at $T = 0.34385$ in the bottom of Fig. 4.9 shows PDC even though $\partial(-\omega_I)/\partial E < 0$. Our statement is only for NDC, and we do not attempt to make any concrete statement for PDC. However, we can make the following discussions. Since our system is neutral, the possible origins of the charge carriers are the following three processes: i) thermal excitation of carriers from the vacuum, ii) the Schwinger effect induced by the electric field that creates pairs of positive and negative charge carriers, and iii) the ionization of the (already-existing) bound states by the electric field. Fig. 4.11 shows the relationship between these

processes. What we have found is that when NDC is realized, the main origin of the charge carriers is iii). However, the above three processes can contribute to the electric conduction in general. For example, when we raise the temperature, the process i) will not be negligible. This implies that the mechanism of NDC we proposed above will not work in the high-temperature region. Indeed, the system shows the $J$-$E$ characteristics given by $J \approx \mathcal{N}E^{3/2}$, which gives PDC, at the high-temperature limit. Therefore, we should consider not only the process iii) but also others for PDC.

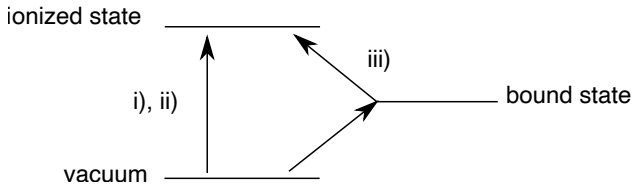


Figure 4.11: Schematic picture of three processes to produce charge carriers. We consider three states: vacuum state without particles, the bound state and the ionized state. The processes, i) and ii) are considered as the transition from the vacuum state to the ionized state. iii) corresponds to the decay process of the bound state.

Before closing this section, we make a comment on how to measure the lifetime of the bound states in experiment. We have computed the lifetime of the bound state from the imaginary part of the quasinormal frequency. Alternatively, one can read it from the full width at half maximum (FWHM) of peaks in the $\omega$-dependence of the AC conductivity. Since the AC conductivity is measurable in experiments, it is worth while reviewing how the lifetime comes into the AC conductivity.

Let us assume that the standard oscillator model called the Lorentz model [33] can be applied to our system. In the oscillator model, the dielectric function is given by

$$\epsilon(\omega) = \epsilon_\infty + \sum_n \left[ \frac{-S_n \mathcal{E}_n^2(\omega^2 - \mathcal{E}_n^2)}{(\omega^2 - \mathcal{E}_n^2)^2 + \omega^2\gamma_n^2} + i\frac{S_n\omega\gamma_n\mathcal{E}_n^2}{(\omega^2 - \mathcal{E}_n^2)^2 + \omega^2\gamma_n^2} \right], \tag{4.42}$$

where $S_n$, $\mathcal{E}_n$ and $\gamma_n$ are the oscillator strength, the oscillator frequency and the damping factor of each oscillator labeled by $n$. $\epsilon_\infty$ is the dielectric constant at high frequency. The oscillator frequency and the damping factor corresponds to the energy and the decay width of the bound states, respectively. The AC conductivity is related to the dielectric function by $\sigma(\omega) = -i\omega\epsilon(\omega)$. The real part of the AC conductivity is expressed as

$$\mathrm{Re}\sigma(\omega) = \sum_n \frac{S_n\omega^2\gamma_n\omega_n^2}{(\omega^2 - \omega_n^2)^2 + \omega^2\gamma_n^2}. \tag{4.43}$$

$\mathrm{Re}\sigma(\omega)$ has a peak at $\omega = \omega_n$ when $\gamma_n/\omega_n$ is sufficiently small. $\gamma_n$ is the FWHM of each peak centering at $\omega = \omega_n$.

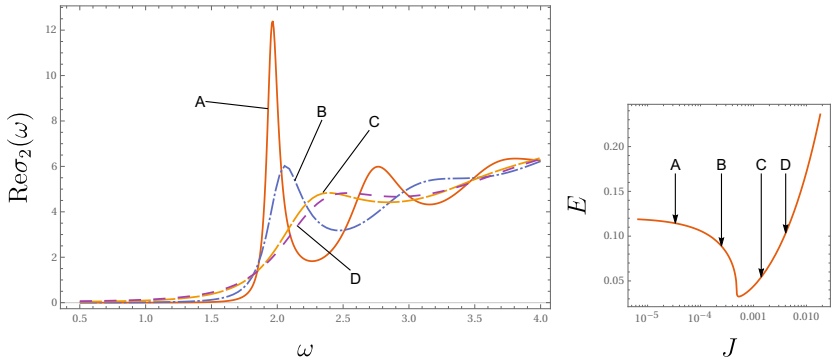


Figure 4.12: (Left) AC conductivity, (Right) $J$-$E$ characteristic at $T = 0.34364$.[13] The value of $J$ for each curve in the left figure correspond to those labeled by A to D on the $J$-$E$ curve.

In our gravity model, the AC conductivity can be calculated by using (4.32).[6] Figure 4.12 shows the real part of the AC conductivity at $T = 0.34364$ for various $J$ in our system. The spectrum of the AC conductivity has peaks. We can see the peak located at $\omega \approx 2$ broadens as $J$ increases along the curve in the right figure of Fig. 4.12. This behavior is consistent with our result shown in Fig. 4.9 at $T = 0.34364$ that $-\omega_I$ of the lowest mode increases when $J$ grows.

[6]The spectrum function corresponding to the AC conductivity in this setup has been investigated in [29].

# Chapter 5

# Ohter applications of the analysis of QNM

In this chapter, we present other applications of the analysis of QNM in the D3-D7 model.

First, we discuss a setup for the analysis of linear stability of the system in the NDC regime when we control $E$. Since the $J$-$E$ characteristic is a multi-valued function of $E$, we expect that the system will be unstable if we allow fluctuation of $J$. This instability will be observed by considering the perturbation field of $A_1(x)$ along the direction of $J$.

Second, we show the existence of the Nambu-Goldstone mode associated with the spontaneous breaking of the $\mathrm{U}(1)_R$ chiral symmerty from the gravity model.[14][1] The D3-D7 model exhibits the magnetic catalysis when we apply external magnetic field. At finite temperature, the system is an open system which has a contact with the heat bath. We show the dispersion relation of the Nambu-Goldstone mode in this open system.

## 5.1 Linear stability of the holographic conductor

In this section, we consider the linear stability of the holographic conductor. The setup is the same as Section 3.3. We apply electric field along $x^1$ direction to the system and the charge density of the system is zero. In order to see the stability of the system, we consider the perturbation field of $A_1$. Unlike $A_\perp$, $A_1$ is coupled with the scalar field $\theta$. So, we employ the following ansatz:

$$A_a \mathrm{d}\xi^a = (-Et + a_1(z))\mathrm{d}t + \mathcal{A}_1(t,z)\mathrm{d}x^1, \quad \theta = \bar{\theta}(z) + \vartheta(t,z), \tag{5.1}$$

where $\mathcal{A}_1(t,z)$ and $\vartheta(t,z)$ represent perturbation fields. $a_1(z)$ and $\tilde{\theta}(z)$ are the background solutions of (3.39) and (3.46), respectively. The equation we will

[1] This work is based on a collaboration with M. Matsumoto.

solve is given by linearizing (A.5). Since the expression is lengthy, we don't write them explicitly here. Alternatively, it is formally written as

$$\mathfrak{L}(t,z)\begin{bmatrix}\mathcal{A}_1(t,z)\\ \vartheta(t,z)\end{bmatrix}=0, \tag{5.2}$$

where $\mathfrak{L}(t,z)$ is a second-order linear differential operator which has $2\times 2$ components. We would like to obtain QNMs associated with these perturbation fields. We focus on the case with $E, J>0$. Here, we write $\mathcal{A}_1(z)$ and $\vartheta(z)$ as the Fourier transform of the original fields. By performing Frobenius expansion at $z=z_*$:

$$\begin{bmatrix}\mathcal{A}_1(z)\\ \vartheta(z)\end{bmatrix}=(1-z/z_*)^{\lambda}\begin{bmatrix}\hat{\mathcal{A}}_1(z)\\ \hat{\vartheta}(z)\end{bmatrix}, \tag{5.3}$$

we find one of the Frobenius exponents is $\lambda=0$. As $A_\perp$, $\lambda=0$ corresponds to the ingoing-wave solutions. We formally write the solutions as

$$\begin{bmatrix}\mathcal{A}_1(z)\\ \vartheta(z)\end{bmatrix}=\Pi(z,z_*;\omega)\begin{bmatrix}\mathcal{A}_1(z_*)\\ \vartheta(z_*)\end{bmatrix}, \tag{5.4}$$

where $\Pi(z,z_*;\omega)$ denotes the matrix generating the regular solutions from the fields at $z=z_*$ for given $\omega$. According to [34], the normalizable condition for the coupled perturbation fields is given by

$$\lim_{\varepsilon\to 0}\varepsilon^{-(\Delta_-^{\mathcal{A}_1}+\Delta_-^{\vartheta})}\det\Pi(\varepsilon,z_*;\omega)=0, \tag{5.5}$$

where $\Delta_-$ can be read from the asymptotic expansion of the field as:

$$\phi(z)=\phi_{(0)}z^{\Delta_-}+\phi_{(+)}z^{\Delta_+}+\cdots. \tag{5.6}$$

For $\mathcal{A}_1$ and $\vartheta$, it is given by $\Delta_-^{\mathcal{A}_1}=0$ and $\Delta_-^{\vartheta}=1$, respectively. By using this condition, we analyze the QNMs from the perturbation fields, as those in Section 4.1. From the quasinormal frequency of the QNM, we study the stability of the system against the perturbation of $J$ and $\langle\bar{\psi}\psi\rangle$.

Currently, the author is analyzing the behavior of the QNM in detail. The results will be reported in other literature.[2]

## 5.2 Nambu-Goldstone mode in a holograhic magnetic catalysis

The D3-D7 model has $\mathrm{U}(1)_R$ chiral symmetry for massless case. In Ref. [15, 16], spontaneous breaking of the chiral symmetry in the presence of the external magnetic field has been studied. [3] This is considered as a holographic realization

[2]This work is based on a collaboration with S. Nakamura, S. Kinoshita, M. Matsumoto and Y. Fukazawa.

[3]In Ref. [15, 16], they considered Kalb-Ramond $B$-field. The $B$-field acts as an external magnetic field on the D7-brane's worldvolume.

The phase diagrams of this system in the temperature density (or chemical potential) plane has been studied in Ref. [30].

of the magnetic catalysis in QCD. The spontaneous chiral symmetry breaking ($\chi$SB) gives a massless Nambu-Goldstone (NG) mode. We investigate the dispersion relation of the NG mode by using the QNM analysis. In the Minkowski embeddings, this is given by an ordinary massless mode which has the dispersion relation of $\omega = \pm v|\vec{k}|$.[35] In the black hole embeddings, we find the nontrivial dispersion relation of the NG mode in the open system.[4]

Let us consider the background configuration of the D3-D7 model. The background geometry is Schwarzschild $AdS_5 \times S^5$ (3.33). The action for the D7-brane is given by the DBI action (2.9). We apply a magnetic field along $x^3$ direction to the system with finite density. We employ the following ansatz of the gauge field.

$$A_a \mathrm{d}\xi^a = a_t(z)\mathrm{d}t + Bx^1\mathrm{d}x^2, \tag{5.7}$$

where $B$ is the magnetic field and $a_t(z)$ corresponds to the charge density. Notice that we do not consider applying an electric field, here. The system is open but in equilibrium. The action is written as

$$S_{\mathrm{D7}} = -\mathcal{N}\int \mathrm{d}^4x\mathrm{d}z \cos^3\theta(z)\sqrt{g_{xx}\left(B^2+g_{xx}^2\right)\left(|g_{tt}|g_{zz}-a_t'(z)^2\right)}. \tag{5.8}$$

The constant of motion for $a_t(z)$ is regarded as the charge density $D$. This is given by

$$D = \frac{\partial \mathcal{L}_{\mathrm{D7}}}{\partial a_t'(z)} = -\mathcal{N}\frac{\cos^3\theta(z) g_{xx}(B^2+g_{xx}^2)a_t'(z)}{g_{xx}\left(B^2+g_{xx}^2\right)\left(|g_{tt}|g_{zz}-a_t'(z)^2\right)}, \tag{5.9}$$

where $\mathcal{L}_{\mathrm{D7}}$ is defined by $S_{\mathrm{D7}} = \int \mathrm{d}^4x\mathrm{d}z\mathcal{L}_{\mathrm{D7}}$. By solving this equation for $a_t'(z)$, we obtain

$$a_t'(z) = D\sqrt{\frac{|g_{tt}|g_{zz}}{D^2+\mathcal{N}^2 g_{xx}(B^2+g_{xx}^2)\cos^6\theta(z)}}. \tag{5.10}$$

The non-normalizable mode of $A_t$ is read as the chemical potential which is given by

$$\mu = \lim_{z\to 0} A_t = \int_0^{z_h} a_t'(z)\mathrm{d}z. \tag{5.11}$$

We have set $A_t(z_h)$ to zero. By performing Legendre transformation, we write

$$\begin{aligned}\tilde{\mathcal{L}}_{\mathrm{D7}} =& \mathcal{L}_{\mathrm{D7}} - A_t'(z)\frac{\partial \mathcal{L}_{\mathrm{D7}}}{\partial A_t'(z)} \\ =& -\sqrt{|g_{tt}|g_{zz}}\sqrt{D^2+\mathcal{N}^2 g_{xx}(B^2+g_{xx}^2)\cos^6\theta(z)}.\end{aligned} \tag{5.12}$$

The equation of motion for the embedding function $\theta(z)$ is obtained from (5.12). The thermodynamical stability of the system in this setup have been studied in [30]. For finite $B$ and massless cases, the system exhibits three types of phases as shown in Fig. 5.1: the chiral symmetry restored ($\chi$SR) phase in black hole embeddings, the $\chi$SB phase in black hole embeddings and $\chi$SB phase in Minkowski embeddings. The system in the former two phases has melting bound

[4] In [14], we also find the dispersion relation of the NG mode in NESS.

states as the QNMs. The system in the last phase has bound states with infinite lifetimes as the normal modes. The order parameter of the chiral symmetry is the chiral condensate $\langle \bar{q}q \rangle$. This field theory's quantity corresponds to bending of the probe brane in this model. So, the $\chi$SR phase corresponds to the flat embedding which is given by $\theta(z) = 0$. Fig. 5.2 shows the phase diagram in $\mu$-$T$ plane. This phase diagram is obtained by computing the grand potential: $\Omega(T, \mu) = -S_{\rm D7}/\mathcal{N}$.[30]

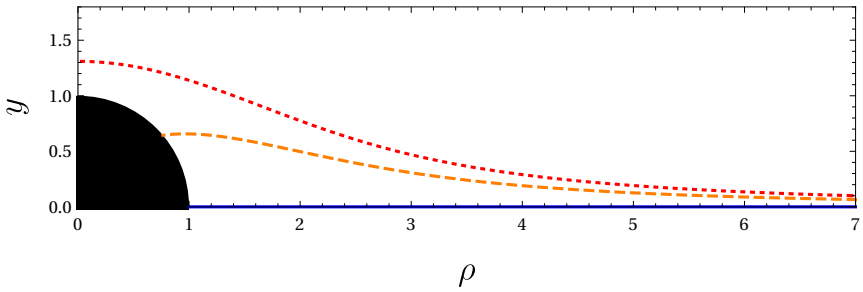


Figure 5.1: Configurations of the brane embeddings for $m_q = 0$. The dotted red line is a Minkowski embedding which represents the $\chi$SB phase. The dashed orange line is a black hole embedding which represents the $\chi$SB phase. The blue line is a black hole embedding which represents the $\chi$SR phase.

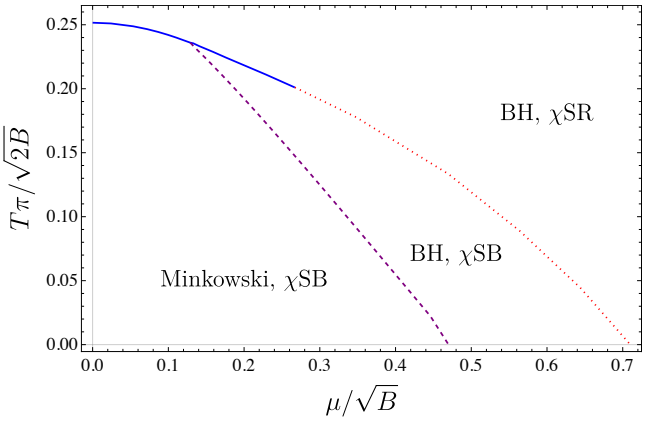


Figure 5.2: Phase diagram in $\mu$-$T$ plane.[30] The dotted line indicates the location where second order transitions occur. The solid line represents the first order transitions.

Let us consider the perturbation fields corresponding to the NG mode of the chiral symmetry. The U(1) chiral transformation corresponds to the SO(2) rotation of the D7-brane in $w_5$-$w_6$ plane. Therefore, the angular coordinate $\psi$ must be corresponding to the NG mode. Note that $\psi$ is coupled with the vector

fields via WZ term of the DBI action. The relevant term is written as

$$S_{\rm WZ} \simeq {\rm Vol}(S^3)\frac{\tau_7}{8}\int {\rm d}^4x{\rm d}z\epsilon^{ijklm}\cos^4\theta\partial_i\psi F_{jk}F_{lm}, \tag{5.13}$$

where $i,j,k\cdots$ denote $\xi^i = t, x^1, x^2, x^3, z$. Now, we consider the following ansatz for the perturbation fields:

$$\psi = 0 + \delta\psi(t, x^\perp, z), \quad A_3 = \delta A_3(t, x^\perp, z), \tag{5.14}$$

where $x^\perp = x^1$ or $x^2$. We assumed the perturbation fields are independent of $x^3$ for simplicity. Expanding the action to quadratic order in $\delta\psi$ and $\delta A_3$, we obtain the equations of motion for the fluctuations:

$$\begin{aligned} &\partial_a\sqrt{-\det G_{ab}}\gamma^{ab}g_{\psi\psi}\partial_b\delta\psi - (\cos^4\theta)'B\partial_t\delta A_3 = 0, \\ &-2\partial_a\sqrt{-\det G_{ab}}\gamma^{ab}g^{33}\partial_{[b}\delta A_{3]} + (\cos^4\theta)'B\partial_t\delta\psi = 0, \end{aligned} \tag{5.15}$$

where $G_{ab} = g_{ab} + F_{ab}$. By performing Fourier transformation, we obtain

$$\begin{aligned} &\partial_z\left[\sqrt{-\det G_{ab}}g_{\psi\psi}\gamma^{zz}\partial_z\delta\psi(z)\delta\psi(z)\right] \\ &\quad - k_\alpha k_\beta\sqrt{-\det G_{ab}}g_{\psi\psi}\gamma^{\alpha\beta}\delta\psi(z) + i\omega(\cos^4\theta)'B\delta A_3(z) = 0, \\ &\partial_z\left[\sqrt{-\det G_{ab}}g^{33}\gamma^{zz}\partial_z\delta A_3(z)\right] \\ &\quad - k_\alpha k_\beta\sqrt{-\det G_{ab}}g^{33}\gamma^{\alpha\beta}\delta A_3(z) + i\omega(\cos^4\theta)'B\delta\psi(z) = 0, \end{aligned} \tag{5.16}$$

where $\alpha,\beta = t, x^\perp$. Note that $\gamma^{ab}$ is diagonal in the present case. We simply wrote $\delta\psi(z)$ and $\delta A_3(z)$ as the Fourier transformations of the original perturbation fields. The ingoing-wave boudary condition at $z = z_h$ is imposed as the following redefinitions:

$$\delta\psi(z) = (1 - z/z_h)^{-i\omega/2\pi T}\delta\tilde{\psi}(z), \quad \delta A_3(z) = (1 - z/z_h)^{-i\omega/2\pi T}\delta\tilde{A}_3(z). \tag{5.17}$$

We find the QNMs of the these coupled fluctuations by using the condition (5.5). In order to avoid a coordinate singularity appearing when $\theta(z) = 0$, we shall use $\delta w(z) \equiv z\delta\psi(z)/\sin\theta(z)$ rather than $\delta\psi(z)$ itself. Then, the values of $\Delta_-$ are given by zero for $\delta w(z)$ and $\delta A_3(z)$. The dispersion relation of the corresponding mode is given by the quasinormal frequency as a function of the spatial momentum $k_\perp$.

Figure 5.3 shows the dispersion relations for the lowest two modes corresponding to the perturbation field of $\psi$ and $A_3$. In each plot, filled circles and open circles denote the real part and the imaginary part of $\omega/\sqrt{B}$, respectively. In the chiral symmetry restored phase (upper left), the perturbation fields of $\psi$ (scalar) and $A_3$ (vector) are decoupled from each other. The both modes are observed as the purely imaginary modes. In the chiral symmetry broken phase, however, these perturbation fields are coupled with each other, as discussed above, then the two modes are mixed. For larger $D/B^{3/2}$ (upper right or lower

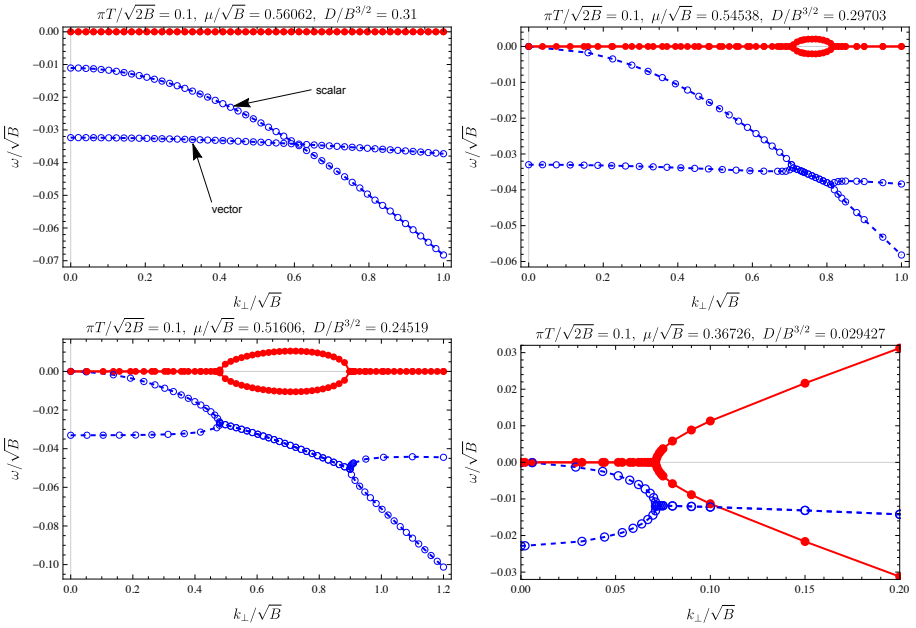


Figure 5.3: The behavior of the real part (filled circles) and the imaginary part (open circles) of $\omega/\sqrt{B}$ as a function of $k_\perp/\sqrt{B}$. In the upper left panel, the system preserves the chiral symmetry and there is no gapless mode. The fluctuations for the scalar field and the vector field (gauge field) are decoupled from each other. In the other panels, the system spontaneously breaks the symmetry and the gapless mode arises.

left), one can see that there are two types of the modes in the small momentum. One of the modes shows zero frequency when the momentum becomes zero, say gapless mode. Another one has finite imaginary part of the frequency at $k_\perp = 0$, say gapped mode. As can be seen from Fig. 5.3, the gapless mode behaves as the diffusive mode near zero momentum: $\omega = -iD_\perp k^2$ ($D_\perp$ is a real positive constant). This diffusive behavior of the NG mode in the dissipative system is consistent with that studied in [36, 37]. At specific momentum, these two purely imaginary modes are located at a same point on the imaginary axis of $\omega$, then the real parts are growing. In other words, the hydrodynamic diffusive behavior is changed into the reactive regime. These modes are symmetric under the flipping sign of the real part of the frequencies. Such a behavior of the dispersion relation is called as *k-gap* [38], because there is a gap opening in spatial momentum. *k-gap* is often observed in dissipative quantum systems. As we increase $k_\perp/\sqrt{B}$, the two modes are changed into two purely imaginary modes, again. This long wave-length behavior is similar to the Mott-Ioffe-Regel limit in a crystal, but our system is homogeneous. It is expected that the finite density configuration gives a similar effect in present case.

We found the dispersion relation of the NG mode which agrees with the result in the effective field theory. The QNM analysis allows us to analyze the degrees of freedom in the low-energy physics such as the NG mode.

# Chapter 6

# Summary

In this thesis, we analyzed the lifetime of the bound states by using AdS/CFT correspondence to reveal the mechanism of NDC. We found that the lifetime of the bound states becomes longer as the electric field increases when the system shows NDC. We also found that the charge carriers in our system is mainly produced by the ionization process of the bound states in the parameter region where NDC is realized. These observations lead us to the conclusion that the origin of the NDC in the present system is suppression of the ionization of the bound states which provides the charge carriers, by the increase of the electric field.

We would also like to make a comment on possible connection to experiments. The bound states in the present system correspond to the excitons in the electron-hole systems in the context of solid state physics. It is interesting to see the electric-field dependence of the lifetime of the excitons in the materials which show NDC, experimentally. The lifetime of excitons can be experimentally detected by observing the optical conductivity (AC conductivity). We have presented a short review on the relationship between the lifetime of the bound states and the optical conductivity in Section 4.2.3. Another interesting topic is exciton Bose-Einstein condensation. It has been discussed that excitons may from the exciton Bose-Einstein condensation at low temperatures [39]. It is worthwhile studying how the exciton Bose-Einstein condensation affects the non-linear conductivity of the materials.

We also provided two other applications of the analysis of QNMs. The analysis allows us to compute various properties of the two-point functions in the dual theory, especially the location of the pole. QNMs in the gravity theory gives us important information on the dual field theory which we cannot analyze easily in the conventional method.

# Acknowledgements

I would like to express my special appreciation and thanks to my supervisor Professor Shin Nakamura for the continuous support of my Ph.D. research.

I am also grateful to rest of my thesis committee: Professor Yasushi Ishii, Professor Makoto Katori, Professor Takashi Oka and Professor Tokio Matsuyama.

I would like to thank Professor Kenji Yonemitsu for insightful comments on the early stage of this work. I am grateful to Shunichiro Kinoshita for providing expertise on general relativity. I would also like to thank to rest of my collaborators, Masataka Matsumoto and Yuichi Fukazawa. I am thankful to the group members for fruitful discussions.

I would like to thank Professor Johanna Erdmenger and the members of Theoretische Physik III group in Julius-Maximilians-Universität Würzburg for the hospitality during my stay.

The main works in this thesis was supported by the Research Assistant Fellowship of Chuo University. I would like to thank Chuo University for supporting me during my PhD program. Finally, I would like to thank my family for their continuous support and encouragement to me.

# Appendix A

# Equations of motion and open string metric on D7-brane

In this appendix, we review the basics of the worldvolume theory of D-branes, especially on the derivation of the equation of motion from the DBI action and on the open string metric. The open string metric play a role of an effective metric for the fields on the D-brane. We show the components of the open string metric for our setup, explicitly.

## A.1 Equations of motion

We derive the general expression of the equations of motion for the scalar fields and the vector fields on the D$p$-brane. The DBI part of the D$p$-brane's action is written as

$$S_{\mathrm{D}p} = -\frac{\tau_p}{g_s}\int \mathrm{d}^{p+1}\xi e^{-\phi}\sqrt{-\det(g_{ab}+F_{ab})}, \tag{A.1}$$

where

$$g_{ab} = g_{MN}\partial_a X^M \partial_b X^N \tag{A.2a}$$
$$F_{ab} = \partial_a A_b - \partial_b A_a. \tag{A.2b}$$

The variation of the action with respect to $X^M$ and $A_a$ is given by

$$\delta S_{\mathrm{D}p} = \frac{1}{2}\frac{\tau_p}{g_s}\int \mathrm{d}^{p+1}\xi e^{-\phi}\sqrt{-\det G_{ab}}\left(G^{(ab)}\delta g_{ba} + G^{[ab]}\delta F_{ba}\right). \tag{A.3}$$

where $G_{ab} \equiv g_{ab} + F_{ab}$ and $G^{ab}$ is its inverse matrix. By omitting the surface terms, we obtain

$$\begin{aligned}\delta S_{\mathrm{D}p} = \frac{\tau_p}{g_s}\int \mathrm{d}^{p+1}\xi \Bigg[ \Big( & \partial_a e^{-\phi}\sqrt{-\det G_{ab}}G^{(ab)}g_{MN}\partial_b X^N \\ & + \frac{1}{2}e^{-\phi}\sqrt{-\det G_{ab}}G^{(ab)}\frac{\partial g_{PQ}}{\partial X^M}\partial_a X^P \partial_b X^Q\Big)\delta X^M \\ & + \Big(\partial_b e^{-\phi}\sqrt{-\det G_{ab}}G^{[ab]}\Big)\delta A_a\Bigg].\end{aligned} \tag{A.4}$$

By using (A.9), we obtain the equations of motion:

$$\begin{aligned}\partial_a e^{-\phi}\sqrt{-\det G_{ab}}\gamma^{ab}g_{MN}\partial_b X^N & \\ + \frac{1}{2}e^{-\phi}\sqrt{-\det G_{ab}}\gamma^{ab}\frac{\partial g_{PQ}}{\partial X^M}\partial_a X^P\partial_b X^Q = 0, & \qquad \text{(A.5a)} \\ \partial_b e^{-\phi}\sqrt{-\det G_{ab}}g^{ac}F_{cd}\gamma^{ab} = 0, & \qquad \text{(A.5b)}\end{aligned}$$

where $\gamma^{ab} = G^{(ab)}$ is the inverse matrix of the open string metric. So far, we have omitted the WZ term. When WZ term contributes, we must add its contribution to (A.5).

## A.2 Open string metric

The inverse matrix of $G_{ab}$ can be written as

$$G^{-1} = (I + g^{-1}F)^{-1}g^{-1} = \sum_{k=0}^{\infty}(-g^{-1}F)^k g^{-1}. \tag{A.6}$$

The symmetric part of $G^{-1}$ is written as

$$\frac{G^{-1} + (G^{-1})^T}{2} = \sum_{k=0}^{\infty}(g^{-1}F)^{2k}g^{-1} = (g - Fg^{-1}F)^{-1}. \tag{A.7}$$

The anti-symmetric part is given by

$$\frac{G^{-1} - (G^{-1})^T}{2} = -\sum_{k=0}^{\infty}(g^{-1}F)^{2k+1}g^{-1} = g^{-1}F(g - Fg^{-1}F)^{-1}. \tag{A.8}$$

So we have the relationship:

$$G^{[ab]} = g^{ac}F_{cd}G^{(db)}. \tag{A.9}$$

The open string metric is defined by

$$\gamma_{ab} = g_{ab} - F_{ac}g^{cd}F_{db}. \tag{A.10}$$

The inverse of the open string metric agree with (A.7).

Let us write the components of the open string metric, explicitly. In Section 4.1, we employed the ansatz for the background vector fields as

$$A_a \mathrm{d}\xi^a = (-Et + a_1(z))\mathrm{d}x^1. \tag{A.11}$$

Then, the open string metric is written as

$$\gamma_{ab} = \begin{bmatrix} -|g_{tt}| + \frac{E^2}{g_{xx}} & 0 & 0 & 0 & -\frac{EA_1'}{g_{xx}} \\ & -\frac{E^2}{|g_{tt}|} + g_{xx} + \frac{A_1'^2}{g_{zz}} & 0 & 0 & 0 \\ & & g_{xx} & 0 & 0 \\ & & & g_{xx} & 0 \\ & & & & g_{zz} + \frac{A_1'^2}{g_{xx}} \end{bmatrix} \\ \oplus \mathrm{diag}\left(\cos^2\theta, \cos^2\theta, \cos^2\theta\right) \tag{A.12}$$

Here, we made abbreviation without displaying the lower-left components, since they are the same as the upper-right components. The components of the inverse metric is given by

$$\gamma^{ab} = \begin{bmatrix} \frac{-g_{xx}^2(A_1'^2 + g_{xx}g_{zz})}{R(z)} & 0 & 0 & 0 & -\frac{EA_1'g_{xx}^2}{R(z)} \\ & \frac{|g_{tt}|g_{xx}^2 g_{zz}}{R(z)} & 0 & 0 & 0 \\ & & \frac{1}{g_{xx}} & 0 & 0 \\ & & & \frac{1}{g_{xx}} & 0 \\ & & & & -\frac{g_{xx}^2 h(z)}{R(z)} \end{bmatrix} \\ \oplus \mathrm{diag}\left(\frac{1}{\cos^2\theta}, \frac{1}{\cos^2\theta}, \frac{1}{\cos^2\theta}\right), \tag{A.13}$$

where $h(z)$ is defined in (3.40) and $R(z)$ is given by

$$R(z) = \frac{-\det(g_{ab} + F_{ab})}{\cos^6\theta(z)} = g_{xx}^2\left(|g_{tt}|A_1'(z)^2 - g_{zz}h(z)\right). \tag{A.14}$$

Again, we made abbreviated in (A.13).

# Appendix B

# Real part of the quasinormal frequencies

In this appendix, we show the real part of the quasinormal frequencies as a function of the constant electric field in the setup of Section 4.1.

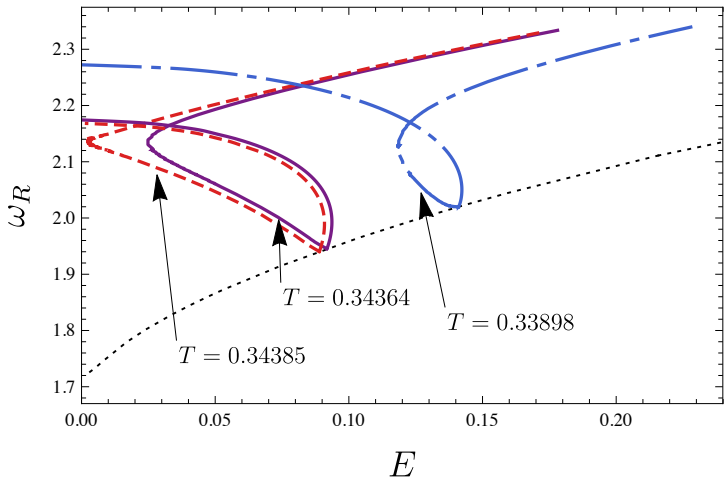


Figure B.1: The real part of the (quasi)normal frequencies of the lowest modes as a function of $E$ at various temperatures. The border between the insulator phase (Minkowski embedding) and the conductor phase (black hole embedding) is the point where the curve touches the dotted line. On the dotted line, $\omega_R$ of the lowest QNM agrees with the normal frequency of the lowest normal mode.

Figure B.1 shows the relation between the real part of the lowest (quasi)normal frequencies as a function of the constant electric field. In this figure, we showed both of the results in the conductor phase and the insulator phase. The border

between the insulator phase and the conductor phase is the point where each curves touches the dotted line and the data are divided into two branches there. At $T = 0.33898$ and $T = 0.34364$, the data from $E = 0$ to the point on the dotted line correspond to the insulator phase. Another part of each curve corresponds to the conductor phase. The curves are smoothly connected except the border of the phases. At $T = 0.34385$, there are two branches which extend from $E = 0$ to the point on the dotted line. In this case, the upper branch corresponds to the insulator phase. The lower branch and the anothe branch from $E = 0$ are correspond to the conductor phase.

In the insulator phase, the normal mode has real valued frequency and $\omega_I = 0$. The bound state is not melting. For large enough $E$, the insulation is broken. Then, the imaginary part of the quasinormal frequency becomes to be non-zero as shown in Fig. 4.9. Unlike Fig. 4.7, $\omega_R$ converges at the border of both phases in this configuration.

# Bibliography


[1] H. Aoki, N. Tsuji, M. Eckstein, M. Kollar, T. Oka, and P. Werner, "Nonequilibrium dynamical mean-field theory and its applications", Reviews of Modern Physics **86**, 779 (2014).

[2] J. M. Maldacena, "The large N limit of superconformal field theories and supergravity", Adv. Theor. Math. Phys. **2**, 231 (1998), arXiv:hep-th/9711200.

[3] S. S. Gubser, I. R. Klebanov, and A. M. Polyakov, "Gauge theory correlators from non-critical string theory", Phys. Lett. B **428** (1998), arXiv:hep-th/9802109.

[4] E. Witten, "Anti-de sitter space and holography", Adv. Theor. Math. Phys. **2** (1998), arXiv:hep-th/9802150.

[5] S. Nakamura, "Negative differential resistivity from holography", Prog. Theor. Phys. **124**, 1105 (2010), arXiv:1006.4105 [hep-th].

[6] S. Nakamura, "Nonequilibrium phase transitions and a nonequilibrium critical point from anti-de sitter space and conformal field theory correspondence", Phys. Rev. Lett. **109**, 120602 (2012), arXiv:1204.1971 [hep-th].

[7] M. Ali-Akbari and A. Vahedi, "Non-equilibrium phase transition from ads/cft", Nuclear Physics B **877**, 95 (2013).

[8] M. Matsumoto and S. Nakamura, "Critical Exponents of Nonequilibrium Phase Transitions in AdS/CFT Correspondence", Phys. Rev. D **98**, 106027 (2018), arXiv:1804.10124 [hep-th].

[9] T. Imaizumi, M. Matsumoto, and S. Nakamura, "Current Driven Tricritical Point in Large- $N_c$ Gauge Theory", Phys. Rev. Lett. **124**, 191603 (2020), arXiv:1911.06262 [hep-th].

[10] A. Karch and E. Katz, "Adding flavor to AdS / CFT", JHEP **06**, 043 (2002), arXiv:hep-th/0205236.

[11] A. Karch and A. O'Bannon, "Metallic AdS/CFT", JHEP **09**, 024 (2007), arXiv:0705.3870 [hep-th].

[12] J. Erdmenger, N. Evans, I. Kirsch, and E. Threlfall, "Mesons in gauge/gravity duals - a review", Eur. Phys. J. A **35**, 81 (2008), arXiv:0711.4467 [hep-th].

[13] S. Ishigaki and S. Nakamura, "Mechanism for Negative Differential Conductivity in Holographic Conductors", JHEP **20**, 124 (2020), arXiv:2008.00904 [hep-th].

[14] S. Ishigaki and M. Matsumoto, "Nambu-Goldstone mode in non-equilibrium systems from AdS/CFT correspondence", (2020), arXiv:2012.01177 [hep-th].

[15] V. G. Filev, C. V. Johnson, R. Rashkov, and K. Viswanathan, "Flavoured large N gauge theory in an external magnetic field", JHEP **10**, 019 (2007), arXiv:hep-th/0701001.

[16] J. Erdmenger, R. Meyer, and J. P. Shock, "AdS/CFT with flavour in electric and magnetic Kalb-Ramond fields", JHEP **12**, 091 (2007), arXiv:0709.1551 [hep-th].

[17] M. Natsuume, *AdS/CFT Duality User Guide*, Vol. 903 (2015), arXiv:1409.3575 [hep-th].

[18] M. Ammon and J. Erdmenger, *Gauge/gravity duality: foundations and applications* (Cambridge University Press, 2015).

[19] J. Polchinski, "Dirichlet Branes and Ramond-Ramond charges", Phys. Rev. Lett. **75**, 4724 (1995), arXiv:hep-th/9510017.

[20] I. R. Klebanov and E. Witten, "AdS / CFT correspondence and symmetry breaking", Nucl. Phys. B **556**, 89 (1999), arXiv:hep-th/9905104.

[21] G. T. Horowitz and A. Strominger, "Black strings and P-branes", Nucl. Phys. B **360**, 197 (1991).

[22] S.-J. Rey and J.-T. Yee, "Macroscopic strings as heavy quarks in large N gauge theory and anti-de Sitter supergravity", Eur. Phys. J. C **22**, 379 (2001), arXiv:hep-th/9803001.

[23] S.-J. Rey, S. Theisen, and J.-T. Yee, "Wilson-Polyakov loop at finite temperature in large N gauge theory and anti-de Sitter supergravity", Nucl. Phys. B **527**, 171 (1998), arXiv:hep-th/9803135.

[24] M. Kruczenski, D. Mateos, R. C. Myers, and D. J. Winters, "Meson spectroscopy in AdS/CFT with flavour", JHEP **2003**, 049 (2003), arXiv:hep-th/0304032.

[25] D. Mateos, R. C. Myers, and R. M. Thomson, "Holographic phase transitions with fundamental matter", Phys. Rev. Lett. **97**, 091601 (2006), arXiv:hep-th/0605046.

[26] R. C. Myers, A. O. Starinets, and R. M. Thomson, "Holographic spectral functions and diffusion constants for fundamental matter", JHEP **0711**, 091 (2007), arXiv:0706.0162 [hep-th].

[27] C. Hoyos-Badajoz, K. Landsteiner, and S. Montero, "Holographic meson melting", JHEP **04**, 031 (2007), arXiv:hep-th/0612169.

[28] E. Schöll, *Nonlinear spatio-temporal dynamics and chaos in semiconductors* (Cambridge University Press, Cambridge, 2001).

[29] J. Mas, J. P. Shock, and J. Tarrio, "Holographic spectral functions in metallic AdS/CFT", JHEP **0909**, 032 (2009), arXiv:0904.3905 [hep-th].

[30] N. Evans, A. Gebauer, K.-Y. Kim, and M. Magou, "Holographic Description of the Phase Diagram of a Chiral Symmetry Breaking Gauge Theory", JHEP **03**, 132 (2010), arXiv:1002.1885 [hep-th].

[31] D. T. Son and A. O. Starinets, "Minkowski space correlators in AdS / CFT correspondence: Recipe and applications", JHEP **09**, 042 (2002), arXiv:hep-th/0205051.

[32] M. Kaminski, K. Landsteiner, F. Pena-Benitez, J. Erdmenger, C. Greubel, and P. Kerner, "Quasinormal modes of massive charged flavor branes", JHEP **2010**, 117 (2010), arXiv:0911.3544 [hep-th].

[33] F. Wooten, *Optical properties of solids* (Academic Press, New York, 1972).

[34] M. Kaminski, K. Landsteiner, J. Mas, J. P. Shock, and J. Tarrio, "Holographic operator mixing and quasinormal modes on the brane", JHEP **2010**, 21 (2010), arXiv:0911.3610 [hep-th].

[35] V. G. Filev, C. V. Johnson, and J. P. Shock, "Universal Holographic Chiral Dynamics in an External Magnetic Field", JHEP **08**, 013 (2009), arXiv:0903.5345 [hep-th].

[36] Y. Minami and Y. Hidaka, "Spontaneous symmetry breaking and Nambu-Goldstone modes in dissipative systems", Phys. Rev. E **97**, 012130 (2018), arXiv:1509.05042 [cond-mat.stat-mech].

[37] M. Hongo, S. Kim, T. Noumi, and A. Ota, "Effective Lagrangian for Nambu-Goldstone modes in nonequilibrium open systems", (2019), arXiv:1907.08609 [hep-th].

[38] M. Baggioli, M. Vasin, V. V. Brazhkin, and K. Trachenko, "Gapped momentum states", Phys. Rept. **865**, 1 (2020), arXiv:1904.01419 [cond-mat.stat-mech].

[39] S. A. Moskalenko and D. W. Snoke, *Bose-einstein condensation of excitons and biexcitons: and coherent nonlinear optics with excitons* (Cambridge University Press, New York, 2000).